UiT
THE ARCTIC
UNIVERSITY
OF NORWAY

Faculty of Science and Technology
Department of Mathematics and Statistics

Separable representations of the Poisson, Helmholtz and complex Helmholtz Kernels

—

Magnar Bjørgve

MAT-3900 Master's thesis in applied mathematics
February 2017

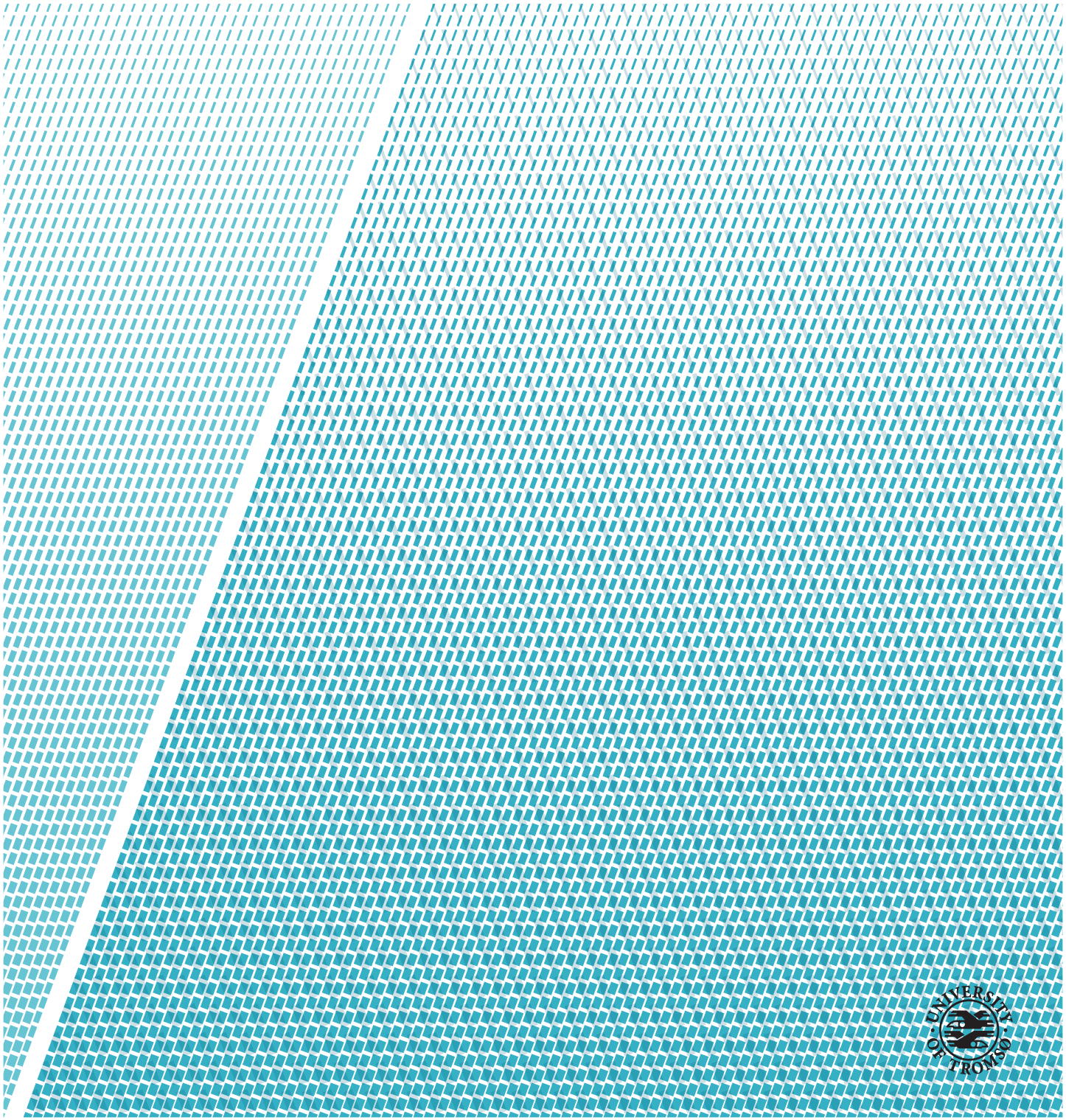

In loving memory of Santo and Ramsi.

“The first law of thermodynamics says that work is indestructable. We who use computers know better”
–Unknown

“Det er jo allmennkunnskap blandt matematikere!”
–Vidar Guddingsmo

Abstract

For high accuracy applications of integral operators in higher dimensions the complexity of operation and storage usually grows exponentially with dimensions. One method that has proven successful for handling these difficulties are the separation of the integral kernels as linear combinations of products of one-dimensional kernels, commonly referred to as separation of variables. In this thesis we optimize the existing separable forms of the Poisson and complex Helmholtz kernels used in the program package MRCPP. We then find a new separable representation of the (non-complex) Helmholtz kernel.

Acknowledgements

I would like to begin with expressing my bottomless gratitude to my supervisors professor Tor Fla and Dr. Stig Rune Jensen. Tor thank you for letting me work on a problem that in the end has expanded my understanding and appreciation of mathematics to a point I never thought possible. Stig thank you for teaching me everything I have needed to know in quantum chemistry and multi resolution analysis to write this thesis, and thank you for taking me with you to the multi resolution analysis summer school at Stony Brook University. And to both of you thank for not giving up on me (and if you did, for not showing it).

A special thanks to the people in the MRChem group, Luca, Peter and Rune. I have enjoyed our weekly group meetings. And I truly hope I will be a part of them in the future.

Furthermore I would like to thank Stony Brook University and the Department of mathematics and statistics at UiT for funding my the trip Stony Brook, NY.

I would also like to thank all of the friends I have gathered through the my years at UiT. Rune, Amund, Thomas, Arja, Elisabeth, Tobias, Lars, Vegard, Irmelin and many many more (I apologise if I forgot your name while writing this).

Most of all, thank you to my family and girlfriend Marit. For supporting me both when I needed it and when I really needed it. I love you all more then any of you can ever imagine.

Special mention and thanks goes to Patrick and Lena McDonnell for proof reading at the early stages of this thesis.

Contents

List of Figures

List of Tables

List of Algorithms

1

Introduction

MRChem [1] is a numerical real-space code for molecular electronic structure calculations within the self-consistent field (SCF) approximations of quantum chemistry. The code is built upon the MultiResolution Computation Program Package (MRCPP), which is a general purpose numerical mathematics library based on multiresolution analysis and the multiwavelet basis which provide low-scaling algorithms as well as rigorous error control in numerical computations.

The work in this thesis contributes to the separable operator representations required in the MRCPP library, where we optimize the already existing separable representations of the Poisson and complex Helmholtz integral kernels, and suggest a new separable representation of the (non-complex) Helmholtz kernel.

1.1 The Kohn-Sham equations

In the Kohn-Sham [2] formulation of Density Functional Theory [3], the many-particle wave function of quantum mechanics is replaced by a set of one-particle orbitals ψ_i interacting through the Kohn-Sham effective potential V_{eff}. The orbitals are obtained as solutions to a set of coupled eigenvalue equations

$$\left(-\frac{1}{2}\nabla^2 + V_{eff}(\mathbf{x})\right)\psi_i(\mathbf{x}) = \epsilon_i\psi_i(\mathbf{x}) \tag{1.1}$$

where the eigenvalues $\epsilon_i < 0$ are often referred to as orbital energies. For a closed-shell (spin unpolarized) molecule we assume double occupancy, and the N electrons of the system are assigned to the $N/2$ orbitals of lowest energy. From this the electronic charge distribution ρ is given by the Kohn-Sham orbitals as

$$\rho(\mathbf{x}) = 2\sum_{i}^{N/2}|\psi_i(\mathbf{x})|^2 \tag{1.2}$$

The effective potential is a collection of the three terms

$$V_{eff}(\mathbf{x}) = V_{nuc}(\mathbf{x}) + V_{el}(\mathbf{x}) + V_{xc}(\mathbf{x}) \tag{1.3}$$

The nuclear potential V_{nuc} accounts for the electrostatic attraction between the electrons and the nuclei, given by the classical expression

$$V_{nuc}(\mathbf{x}) = -\sum_{I=1}^{N_{nuc}}\frac{Z_I}{|\mathbf{x}-\mathbf{x}_I|} \tag{1.4}$$

where Z_I and $\mathbf{x}_I$ are the charges and positions of the nuclei. The electronic potential V_{el} is the classical repulsion between the electrons, and is related to the electronic charge distribution through the Poisson equation

$$-\nabla^2 V_{el}(\mathbf{x}) = 4\pi\rho(\mathbf{x}) \tag{1.5}$$

Finally, the exchange-correlation (XC) potential V_{xc} is the term that accounts for all non-classical quantum effects. In principle, the exact XC potential

would make the Kohn-Sham equations (1.1) equivalent to the many-particle Schrödinger equation, and the Kohn-Sham electronic density would be the exact (non-relativistic) density. However, the exact form of the XC potential is not known, but a large number of approximate XC energy functionals are available, with variable level of complexity and both with and without empirical parameters [4].

1.2 Multiwavelets

Alpert's[5] construction of the multiwavelet basis set can be understood by the following argument. Starting with a small set of polynomials $\{\phi_i\}_{i=0}^{k}$ of order $\leq k$ on the unit interval, we attempt to represent a given function. If this basis turns out to give a poor representation we increase the order k of the basis, and as the order goes to infinity we reach a complete basis for the interval, and thus an exact representation of the function. In multiresolution analysis instead we keep a fixed finite order of the polynomials. Now, if this turns out to give a poor representation of the function, we split the interval into two subintervals, and double the number of basis functions by dilating and translating the original basis into the two subintervals. This process is continued recursively until we have an accurate representation of the function. An *adaptive* representation of a function can be obtained if we are satisfied with the function representation in one of the subintervals, but not the other. In this case we continue the refinement only where it is necessary, based on some local accuracy requirement, which ensures that the computational effort is focussed in regions where the function is rapidly changing.

As shown by Alpert, this construction fits into the theory of wavelets, which means that the basis has several desireable properties, like efficient representation of smooth functions, rigorous error control and sparse representations of certain kinds of integral operators.

A potential problem with this basis set construction is the discontinuities that

arise at the boundaries between different boxes. These lead to high-frequency numerical noise that increase when differential operators are applied. For instance, if we apply the one-dimensinal Laplacian to a function with numerical noise of order ϵ and frequency k

$$\nabla^2(f(x) + \epsilon e^{ikx}) = \nabla^2 f(x) - k^2 \epsilon e^{ikx} \tag{1.6}$$

we see how the differential operators enhances the numerical noise by a factor k^2, leading to large numerical errors for high frequencies. On the other hand, let us consider the *inverse* Laplacian in one dimension

$$\nabla^{-2}(f(x) + \epsilon e^{ikx}) = \nabla^{-2} f(x) - \frac{\epsilon}{k^2} e^{ikx} \tag{1.7}$$

In this case the inverse operator dampens the numerical noise, so that very high accuracy can be maintained. This means that we should seek integral formulations of the Kohn-Sham (1.1) and Poisson (1.5) equations, which can be done if we have the corresponding integral kernels.

For the Poisson equation (1.5), it is simply a matter of inverting the differential operator

$$-\nabla^2 V_{el}(\mathbf{x}) = 4\pi\rho(\mathbf{x}) \tag{1.8}$$

$$V_{el}(\mathbf{x}) = 4\pi P[\rho](\mathbf{x}) \tag{1.9}$$

while the Kohn-Sham equations (1.1) must first be reorganized

$$\left(-\frac{1}{2}\nabla^2 + V_{eff}(\mathbf{x})\right)\psi_i(\mathbf{x}) = \epsilon_i \psi_i(\mathbf{x}) \tag{1.10}$$

$$\left(-\nabla^2 - 2\epsilon_i\right)\psi_i(\mathbf{x}) = -2V_{eff}(\mathbf{x}) \tag{1.11}$$

$$-\left(\nabla^2 - \mu_i^2\right)\psi_i(\mathbf{x}) = -2V_{eff}(\mathbf{x}) \tag{1.12}$$

$$\psi_i(\mathbf{x}) = -2H_c^{\mu_i}\left[V_{eff}\psi_i\right](\mathbf{x}) \tag{1.13}$$

where H_c^{μ} is the complex Helmholtz operator and $\mu_i = \sqrt{-2\epsilon_i}$ are real numbers, assuming negative orbital energies. However, in certain applications this assumption does not hold. For instance, when computing electric properties

as a molecule's response to an external electric field perturbation, we need to invert the following operator

$$\left(-\nabla^2 - 2(\epsilon_i + \omega)\right) g(\mathbf{x}) = f(\mathbf{x}) \tag{1.14}$$

where ω is the frequency of the perturbing field. For low frequencies we can still use the complex Helmholtz operator as defined above, but whenever the orbital energy and the frequency add up to a positive number, we are dealing with the (non-complex) Helmholtz equation

$$-\left(\nabla^2 + \mu_i^2\right) g(\mathbf{x}) = f(\mathbf{x}) \tag{1.15}$$

$$g(\mathbf{x}) = H^{\mu_i}\left[f\right](\mathbf{x}) \tag{1.16}$$

This means that we need representations of the Poisson (P), Helmholtz (H^μ) and complex Helmholtz (H_c^μ) integral kernels in the multiwavelet basis. In most cases the matrix representation of such integral operators will be dense, leading to slow algorithms. However, by the non-standard (NS) form of multiresolution operators presented by Beylkin [6], these kinds of integral operators will have sparse representations in the multiwavelets basis, yielding fast algorithms that scales linearly with the system size. Unfortunately, the straightforward generalization of the NS form to multiple dimensions is too expensive both in application and storage. This again is solved by writing the integral kernels as linear combinations of products of one-dimensional kernels:

$$K(\mathbf{x}, \mathbf{y}) \approx \tilde{K}(\mathbf{x}, \mathbf{y}) \stackrel{\text{def}}{=} \sum_{k=1}^{M} \prod_{p=1}^{d} K_p^k(x_p, y_p) \tag{1.17}$$

By this the storage requirements for the integral operator in a polynomial basis of order k is reduced from

$$O((k+1)^{2d}) \rightarrow O(M(k+1)^2) \tag{1.18}$$

while the complexity of *applying* the operator goes from

$$O((k+1)^{2d}) \rightarrow O(dM(k+1)^{d+1}) \tag{1.19}$$

In (1.17) an exact equality is often not necessary as floating point arithmetic has finite precision. We will seek to bound the pointwise error $e(\mathbf{x})$ where

$$e(\mathbf{x}) \stackrel{\text{def}}{=} \sup_{\mathbf{y}} \left| \frac{K(\mathbf{x},\mathbf{y}) - \tilde{K}(\mathbf{x},\mathbf{y})}{K(\mathbf{x},\mathbf{y})} \right| < \epsilon_s \tag{1.20}$$

The number of terms $M = M_{\epsilon_s}$ in equation (1.17) is called the *separation rank* of K and will depend on ϵ_s. In order to get efficient algorithms for operator applications, M should be as small as possible.

In this thesis we are concerned with two main problems:

1. Reduce the separation rank of the already existing separable representation of the Poisson and complex Helmholtz kernels.

2. Find a separable representation of the (non-complex) Helmholtz kernel.

The rest of the thesis is divided into 5 chapters:

- In chapter 2 we derive the complexity of directly applying an operator in multirsolution analysis (MRA) and how the complexity is reduced for separable operators.

- In chapter 3 we derive the analytic expressons for the Poisson, complex Helmholtz and Helmholtz kernels.

- In chatper 4 we write the Poisson and complex Helmholtz kernels in terms of integrals with superexponentially decaying integrands. We then propose an algorithm designed to find the optimal quadrature range for integrating integrands that decay superexponentially. We then compare our results for the quadrature range of the schemes used in MRChem for the Poisson and compelx Helmholtz kernel.

- In chapter 5 we begin with look at how Beylkin did fast convolutions with the Helmholtz kernel. We then suggest a new separable form of the Helmholtz Kernel.

- In chapter 6 we finish the thesis with a short discussion of our results, we then suggest some future work.

2

Operator projection in MRA

In this chapter do we derive the complexity of direcly applyting an operator in multiresolution analysis (MRA) and how the complexity is reduced for separable operators.

We begin by defining a one-dimensional orthonormal MRA, then expand it to multiple dimensions as a tensor product. We then give an introduction to function and operator projection onto an orthonormal MRA basis.

2.1 Orthonormal multiresolution analysis (MRA)

A multiresolution analysis of $L^2([0,1])$ is an infinite nested sequence of subspaces

$$V_k^0 \subset V_k^1 \subset \ldots \subset V_k^n \subset \ldots \subset L^2([0,1]) \tag{2.1}$$

with the following properties:

1. $\bigcup_{n=0}^{\infty}$ is dense in $L^2([0,1])$
2. $f(x) \in V_k^n \iff f(2x) \in V_k^{n+1}, \forall\, n \in \mathbb{N}$
3. $f(x) \in V_k^n \iff f(x - 2^{-n}l) \in V_k^n \,\forall\, n \in \mathbb{N},\ 0 \leq l \leq 2^n - 1$
4. There exists a function vector Φ in $L^2([0,1])$ of length $k+1$ such that the vector components ϕ_i forms a basis for V_k^0

This means that if Φ spans a basis in V_k^0, containing a finite number of functions $(k+1)$.[1] By property 2 and 3 a basis for V_k^n can be constructed from the basis Φ of V_k^0

$$\phi_{i,l}^n \stackrel{\text{def}}{=} 2^{n/2}\phi_i(2^n x - 1) = \sum_{m=0}^{2^n-1}\sum_{j=0}^{k} H_{j,i}^{(m)}\phi_{j,m}^{n-1}(x) \tag{2.2}$$

where $H^{(m)}$ are the filter matrices that describe the transformation between basis functions in the different spaces V_k^n. The MRA is called orthonormal if

$$\langle \phi_{i,l}^n, \phi_{l,m}^n \rangle = \delta_{i,j}\delta_{l,m} \tag{2.3}$$

This orthonormality condition implies that the basis functions $\phi_{i,l}^n$ are orthonormal both within one function vector and through all possible translations on one scale, but not through different scales. Henceforth when MRA is mentioned its orthonormality is implied.

In figure 2.1, we see an illustration of how the line $[0,1]$ is refined into finer scales. In the figure the grid refinement is uniform, however this is not a requirement.

1. The number k is often referred to as the order of the basis.

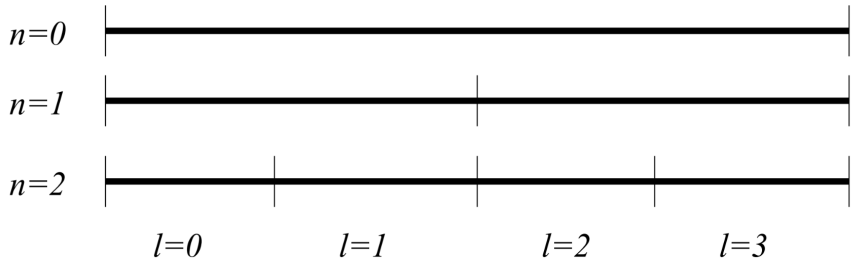

Figure 2.1: One-dimensional *uniform* grid refinement

2.1.1 MRA by tensor products

Now we expand the MRA into multiple dimensions and define the space $V_k^{n,d}$ in terms of a tensor product

$$V_k^{n,d} \stackrel{\text{def}}{=} \bigotimes^{d} V_k^n \tag{2.4}$$

where the spaces V_k^n are defined as multiresolution spaces. The basis for this d-dimensional space is given as tensor products of the one-dimensional basis functions

$$\Phi_{\mathbf{j},\mathbf{l}}^n \stackrel{\text{def}}{=} \prod_{p=1}^{d} \phi_{j_p,l_p}^n(x_p) \tag{2.5}$$

with $0 \leq l_p \leq k$ and $0 < l_p < 2^n - 1$.

The number of basis functions on each hypercube $\mathbf{l} = (l_1, l_2, ..., l_d)$ is $(k+1)^d$, while the number of such hypercubes on scale n becomes 2^{nd}, which means the number of basis functions are growing exponentially with the number of dimensions.

In figure 2.2 we see an example of an *adaptive* grid refinement in three dimensions. This means that basis functions are only projected deeper in places where higher accuracy is required.

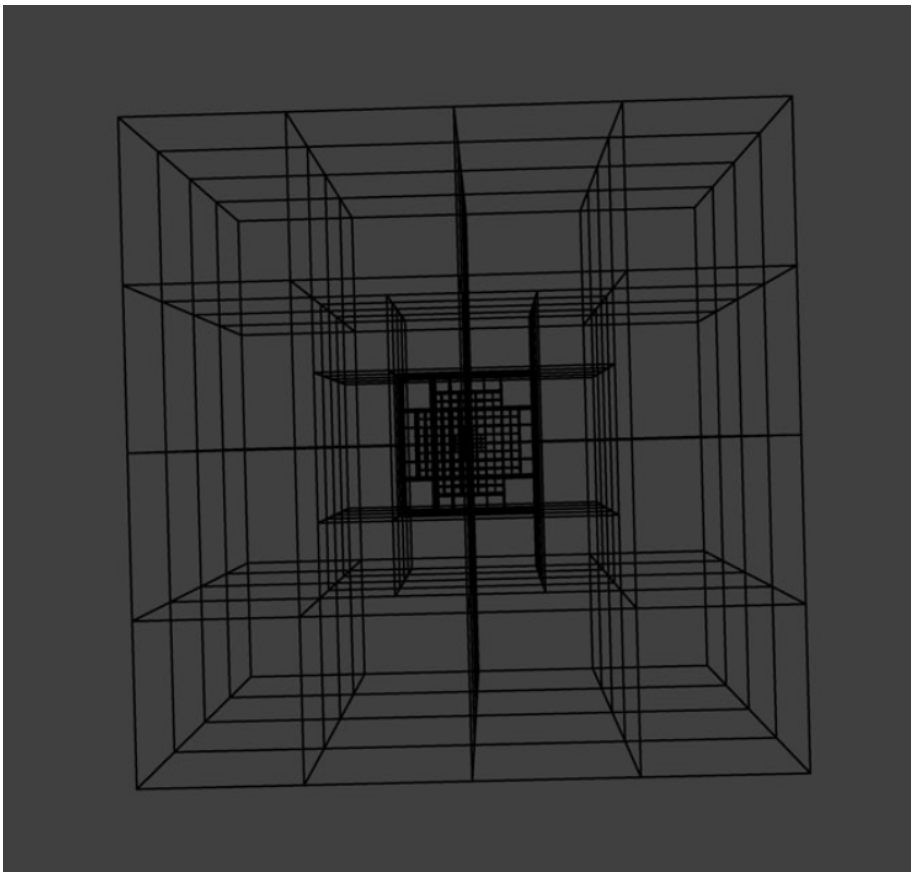

Figure 2.2: Three-dimensional *adaptive* grid refinement

2.2 Function representation

The multi-dimensional function representation is obtained by projecting $f(\mathbf{x})$ onto the multi-dimensional basis $\Phi^n_{\mathbf{j},\mathbf{l}}$ (2.5) that span the space $V_k^{n,d}$

$$f(\mathbf{x}) \approx f^n(\mathbf{x}) = \sum_{\mathbf{l}} \sum_{\mathbf{j}} s^{n,f}_{\mathbf{j},\mathbf{l}} \Phi^n_{\mathbf{j},\mathbf{l}}(\mathbf{x}) \tag{2.6}$$

where the sums are over all possible translation vectors $\mathbf{l} = (l_1, l_2, \ldots, l_p, \ldots, l_d)$ for $0 \leq l_p \leq 2^n - 1$, and all possible basis function combinations $\mathbf{j} = (j_1, j_2, \ldots, j_p, \ldots, j_d)$ for $0 \leq j_p \leq k$. The expansion coefficients $s^{n,f}_{\mathbf{j},\mathbf{l}}$ are obtained by the integral

$$s^{n,f}_{\mathbf{j},\mathbf{l}} = \int f(\mathbf{x}) \Phi^n_{\mathbf{j},\mathbf{l}} \, \mathrm{d}\mathbf{x} \tag{2.7}$$

The accuracy of $f^n(\mathbf{x})$ is determined by the scale n of which the projection is performed, as well as the order k of the basis.

2.3 Operator representation

In this section we describe how to project and apply an integral operator (kernel) in an MRA basis. First by directly projecting the full $2d$-dimensional operator, then we project an operator that can be separated into d two-dimensional contributions. Then we discuss the complexity of these operations and compare the efficiency.

2.3.1 Direct application of multi-dimensional integral operators

An integral operator T in d dimensions is defined by its kernel $K(\mathbf{x}, \mathbf{y})$,

$$[Tf](x) = \int K(\mathbf{x}, \mathbf{y}) f(\mathbf{y}) \, \mathrm{d}\mathbf{y} \tag{2.8}$$

We expand the kernel $K(\mathbf{x}, \mathbf{y})$ in the $2d$-dimensional MRA basis

$$K(\mathbf{x}, \mathbf{y}) \approx K^n(\mathbf{x}, \mathbf{y}) = \sum_{\mathbf{l},\mathbf{m}} \sum_{\mathbf{i},\mathbf{j}} \left[\tau^n_{\mathbf{l}\mathbf{m}}\right]_{\mathbf{i}\mathbf{j}} \Phi^n_{\mathbf{i},\mathbf{l}}(\mathbf{x}) \Phi^n_{\mathbf{j},\mathbf{m}}(\mathbf{y}) \tag{2.9}$$

where the expansion coefficients are given by equation (2.7):

$$\left[\tau^n_{\mathbf{lm}}\right]_{\mathbf{ij}} = \int\int K(\mathbf{x},\mathbf{y})\Phi^n_{\mathbf{i,l}}(\mathbf{x})\Phi^n_{\mathbf{j,m}}(\mathbf{y})\,\mathrm{d}\mathbf{x}\,\mathrm{d}\mathbf{y} \tag{2.10}$$

Inserting (2.9) into (2.8) then yields

$$[Tf]^n(\mathbf{x}) = \int \left(\sum_{\mathbf{l,m}}\sum_{\mathbf{i,j}}[\tau^n_{\mathbf{lm}}]_{\mathbf{ij}}\Phi^n_{\mathbf{i,l}}(\mathbf{x})\Phi^n_{\mathbf{j,m}}(\mathbf{y})\right) f(\mathbf{y})\,\mathrm{d}\mathbf{y} \tag{2.11}$$

$$= \sum_{\mathbf{l,m}}\sum_{\mathbf{i,j}}[\tau^n_{\mathbf{lm}}]_{\mathbf{ij}}\Phi^n_{\mathbf{i,l}}(\mathbf{x}) \int \Phi^n_{\mathbf{j,m}}(\mathbf{y})f(\mathbf{y})\,\mathrm{d}\mathbf{y} \tag{2.12}$$

where we recognize the rightmost integral as the expansion coefficients $s^{n,f}_{\mathbf{j,m}}$ from (2.7). Then the operation $[Tf]^n(\mathbf{x})$ in d dimensions is found to be

$$[Tf]^n(\mathbf{x}) = \sum_{\mathbf{l,m}}\sum_{\mathbf{i,j}}[\tau^n_{\mathbf{lm}}]_{\mathbf{ij}}\Phi^n_{\mathbf{i,l}}(\mathbf{x})s^{n,f}_{\mathbf{j,m}} \tag{2.13}$$

Let us now consider the complexity of this operation. The summation over $\mathbf{l}$ and $\mathbf{m}$ amounts to a prefactor $C(\mathbf{l},\mathbf{m})$ dependent on the scale of refinement and dimension. For a uniform grid refinement this factor would be 2^n for each summation index, e.i. 2^{2dn} in total, where n is refinement level. However, it has been shown that this prefactor can be significantly reduced for appropriately chosen basis sets (multiwavelets in combination with non-standard form of operators) [6], so we omit it in the discussion of complexity here. We see that the number of operations of applying an operator to a function f in an MRA basis is determined by the summation $\sum_{\mathbf{j,i}}$, where we sum over all possible combinations of $\mathbf{j} = (j_1, j_2, \ldots, j_p, \ldots j_d)$ for $0 \leq j_p \leq k$ and $\mathbf{i} = (i_1, i_2, \ldots, i_p, \ldots i_d)$ for $0 \leq i_p \leq k$, yielding a complexity of

$$O((k+1)^{2d}) \tag{2.14}$$

We see that the complexity of applying an operator grows with a power d. This is an example of something commonly dubbed as the *curse of dimensionality*, meaning the operations needed to perform an algorithm increases with a power per dimension.

2.3.2 Separable kernels projected onto an MRA basis

Above we saw how the number of operations needed to apply an integral operator was increased with a power d for each dimension. Here we discuss the complexity of applying operators that can be written in terms of a separable product.

We begin by defining a separable approximation to the kernel

$$K(\mathbf{x}, \mathbf{y}) \approx \tilde{K}(\mathbf{x}, \mathbf{y}) = \sum_{\kappa=1}^{M} \prod_{p=1}^{d} K_p^{\kappa}(x_p, y_p) \tag{2.15}$$

where $\tilde{K}(\mathbf{x}, \mathbf{y})$ is an appropriately[2] accurate representation of $K(\mathbf{x}, \mathbf{y})$. $K_p^{\kappa}(x_p, y_p)$ is the operator kernel in the p-th coordinate, and M is the so-called separation rank of the kernel $\tilde{K}$. An exact equality is often not necessary as floating point arithmetic has finite precision. We will take a closer look at such approximations in chapter 4.

The advantage of a separable representation of the operator is that convolutions can be applied separately in each direction for functions represented in a tensor product basis. In the following we discuss this in detail.

Let

$$[Tf](\mathbf{x}) = \int K(\mathbf{x}, \mathbf{y}) f(\mathbf{y}) \, \mathrm{d}\mathbf{y} \tag{2.16}$$

be an integral operator. We approximate this by

$$[\tilde{T}f](\mathbf{x}) = \sum_{\kappa=1}^{M} \int \prod_{p=1}^{d} K_p^{\kappa}(x_p, y_p) f(\mathbf{y}) \, \mathrm{d}\mathbf{y} \tag{2.17}$$

Next, we project $f(\mathbf{y})$ onto the MRA basis, then insert $f^n(\mathbf{y})$ into equation

2. Piecewise relative error, specified by the user depending on the accuracy sought in the final result.

(2.17)

$$[\tilde{T}f](\mathbf{x}) = \sum_{\kappa=1}^{M} \int \prod_{p=1}^{d} K_p^{\kappa}(x_p, y_p) \sum_{\mathbf{m}} \sum_{\mathbf{j}} s_{\mathbf{j},\mathbf{m}}^{n,f} \Phi_{\mathbf{j},\mathbf{m}}^{n}(\mathbf{y})\, \mathrm{d}\mathbf{y} \tag{2.18}$$

$$= \sum_{\kappa=1}^{M} \sum_{\mathbf{m}} \sum_{\mathbf{j}} s_{\mathbf{j},\mathbf{m}}^{n,f} \int \prod_{p=1}^{d} K_p^{\kappa}(x_p, y_p) \Phi_{\mathbf{j},\mathbf{m}}^{n}(\mathbf{y})\, \mathrm{d}\mathbf{y} \tag{2.19}$$

Writing out the basis $\Phi_{\mathbf{j},\mathbf{m}}^{n}(\mathbf{y}) = \phi_{j_1,m_1}^{n}(y_1) \cdot \phi_{j_2,m_2}^{n}(y_2) \cdot \ldots \cdot \phi_{j_d,m_d}^{n}(y_d)$, and rearranging the integrals, this takes the form

$$\begin{aligned}[\tilde{T}f](\mathbf{x}) = \sum_{\kappa=1}^{M} \sum_{\mathbf{m}} \sum_{\mathbf{j}} s_{\mathbf{j},\mathbf{m}}^{n,f} \Bigg(& \\ & \int K_1^{\kappa}(x_1, y_1) \phi_{j_1,m_1}^{n}(y_1)\, \mathrm{d}y_1 \\ & \int K_2^{\kappa}(x_2, y_2) \phi_{j_2,m_2}^{n}(y_2)\, \mathrm{d}y_2 \ldots \\ & \ldots \int K_p^{\kappa}(x_p, y_p) \phi_{j_p,m_p}^{n}(y_p)\, \mathrm{d}y_p \ldots \\ & \ldots \int K_d^{\kappa}(x_d, y_d) \phi_{j_d,m_d}^{n}(y_d)\, \mathrm{d}y_d \Bigg)\end{aligned} \tag{2.20}$$

Now we take a closer look at the factor

$$\int K_p^{\kappa}(x_p, y_p) \phi_{j_p,m_p}^{n}(y_p)\, \mathrm{d}y_p \tag{2.21}$$

and then project $K_p^{\kappa}(x_p, y_p)$ onto the MRA basis, we get

$$K_p^{\kappa,n}(x_p, y_p) = \sum_{l,l'} \sum_{i,i'} [\tau_{l,l'}^{\kappa,n}]_{ii'} \phi_{i,l}^{n}(x_p) \phi_{i',l'}^{n}(y_p) \tag{2.22}$$

where the expansion coefficients $[\tau_{l,l'}^{\kappa,n}]_{ii'}$ are given by equation (2.10). Inserting (2.22) into equation (2.21) yields

$$\int \sum_{l,l'} \sum_{i,i'} [\tau_{l,l'}^{\kappa,n}]_{ii'} \phi_{i,l}^{n}(x_p) \phi_{i',l'}^{n}(y_p) \phi_{j_p,m_p}^{n}(y_p)\, \mathrm{d}y_p \tag{2.23}$$

$$= \sum_{l,l'} \sum_{i,i'} [\tau_{l,l'}^{\kappa,n}]_{ii'} \phi_{i,l}^{n}(x_p) \int \phi_{i',l'}^{n}(y_p) \phi_{j_p,m_p}^{n}(y_p)\, \mathrm{d}y_p \tag{2.24}$$

By the MRA orthonormality condition (2.3)

$$\int \phi^n_{i',l'}(y_p)\phi^n_{j_p,m_p}(y_p)\,\mathrm{d}y_p = \delta_{i',j_p}\delta_{l',m_p} \tag{2.25}$$

we have

$$\int K^\kappa_p(x_p, y_p)\phi^n_{j_p,m_p}(y_p)\,\mathrm{d}y_p = \sum_{l,m_p}\sum_{i,j_p}[\tau^{\kappa,n}_{l,m_p}]_{ij_p}\phi^n_{i,l}(x_p) \tag{2.26}$$

Using this, we again look at equation (2.20) for $[\tilde{T}f](x)$, which simpifies to

$$[\tilde{T}f](\mathbf{x}) = \sum_{\kappa=1}^{M}\sum_{l=1}^{2^n-1}\sum_{i=0}^{k}\sum_{\mathbf{m}}\sum_{\mathbf{j}} s^{n,f}_{\mathbf{j},\mathbf{m}}\prod_{p=1}^{d}[\tau^{\kappa,n}_{l,m_p}]^p_{i,j_p}\phi^n_{i,l}(x_p) \tag{2.27}$$

Now let us consider the complexity of this operation. Again, the summation over l and m amounts to a prefactor that we omit in the following discussion. We see that the summation $\sum_{\mathbf{j}}$ is to be taken over all possible basis function combinations $\mathbf{j} = (j_1, j_2, \ldots, j_p, \ldots j_d)$ for $0 \leq j_p \leq k$. Giving rise to $(k+1)^d$ operations. Then all of this is summed by $\sum_{i=0}^{k}$ and $\sum_{\kappa=1}^{M}$, adding to the complexity by a factor $(k+1)$ and M, respectively, and the product $\prod_{p=1}^{d}$ adds on a factor d.

Thus, the final number of operations adds up to

$$O(dM(k+1)^{d+1}) \tag{2.28}$$

Clearly, this is not a cure of the curse of dimensionality, however, it makes computations in three dimensions much more manageable. We see that for a sufficiently small separation rank M, the complexity from applying the integral operator is greatly reduced from that of the direct approach.

3

Analytic representations of the free space Poisson, complex Helmholtz and Helmholtz kernel

In this chapter we derive analytic expressions to the free space Poisson, complex Helmholtz and Helmholtz kernels. We follow the apprach by [7] to find the fundamental solutions to the Lapace equation (homogenous Poisson equation), expanding it to yield the fundamental solutions for the complex and non-complex Helmholtz equation. We then require the fundamental solution to have a specific behaviour at boundary, namely zero at infinity. Hence, the fundamental solutions are then the free-space integral kernels of the Poisson, complex Helmholtz and Helmholtz equation.

3.1 Green's identity

For $u, v \in C^2(\bar{\Omega})$ we have Green's identity [7]

$$\int_\Omega v\nabla^2 u \, \mathrm{d}\mathbf{x} = \int_\Omega u\nabla^2 v \, \mathrm{d}\mathbf{x} + \int_{\partial\Omega} \left(v\frac{\mathrm{d}u}{\mathrm{d}\mathbf{n}} - u\frac{\mathrm{d}v}{\mathrm{d}\mathbf{n}} \right) \mathrm{d}S \tag{3.1}$$

where $\frac{\mathrm{d}}{\mathrm{d}\mathbf{n}}$ indicates differentiation in the direction of the exterior normal to $\partial\Omega$.

For $v = 1$ this identity takes the form

$$\int_\Omega \nabla^2 u \, \mathrm{d}\mathbf{x} = \int_{\partial\Omega} \frac{\mathrm{d}u}{\mathrm{d}\mathbf{n}} \, \mathrm{d}S \tag{3.2}$$

It is easy to see that this also holds true for $\nabla^2 + c$, where c is some constant. Thus Green's (3.1) identity can be extended to the in general form

$$\int_\Omega v\mathcal{L}'u \, \mathrm{d}\mathbf{x} = \int_\Omega u\mathcal{L}v \, \mathrm{d}\mathbf{x} + \int_{\partial\Omega} \left(v\frac{\mathrm{d}u}{\mathrm{d}\mathbf{n}} - u\frac{\mathrm{d}v}{\mathrm{d}\mathbf{n}} \right) \mathrm{d}S \tag{3.3}$$

and

$$\int_\Omega \mathcal{L}'u \, \mathrm{d}\mathbf{x} = \int_{\partial\Omega} \frac{\mathrm{d}u}{\mathrm{d}\mathbf{n}} \, \mathrm{d}S \tag{3.4}$$

where $\mathcal{L}' = \nabla^2 + c$.

3.2 Free-space kernels

We begin with considering the problem

$$\mathcal{L}'u(\mathbf{x}) = 0 \tag{3.5}$$

$$u(\mathbf{x}) = 0 \text{ on } \partial\Omega \tag{3.6}$$

where $u(x)$ is of class C^2 in Ω and

$$\mathcal{L}'_L = \nabla^2 \quad \text{Laplace Operator} \tag{3.7}$$

$$\mathcal{L}'_{cH} = \nabla^2 - \mu^2 \quad \text{Complex Helmholtz Operator} \tag{3.8}$$

$$\mathcal{L}'_H = \nabla^2 + \mu^2 \quad \text{Helmholtz Operator} \tag{3.9}$$

μ is a constant greater than zero.

For the Laplace, complex Helmholtz and Helmholtz operators this equation is perserved under rotations about a point $\mathbf{y}$, see Appendix B. This makes it plausible that there exist special solutions $v(\mathbf{x})$ of (3.5) that are invariant under rotations about $\mathbf{y}$, that is have the same value at all points $\mathbf{x}$ at the same distance from $\mathbf{y}$. Such solutions would be of the form

$$v(\mathbf{x}) = K(r) \tag{3.10}$$

where

$$r = |\mathbf{x} - \mathbf{y}| \tag{3.11}$$

we are then lead to the ordinary differential equation

$$\mathcal{L}'K(r) = 0 \tag{3.12}$$

$$K(r) = 0 \text{ as } r \to \infty \tag{3.13}$$

or written out explicitly for each case

$$K_L''(r) + \frac{2}{r}K_L'(r) = 0 \tag{3.14}$$

$$K_{cH}''(r) + \frac{2}{r}K_{cH}'(r) - \mu^2 K_{cH}(r) = 0 \tag{3.15}$$

$$K_H''(r) + \frac{2}{r}K_H'(r) + \mu^2 K_H(r) = 0 \tag{3.16}$$

A solution of (3.14) and its derivative is found to be,

$$K_L(r) = \frac{C}{r} \tag{3.17}$$

$$\frac{\mathrm{d}}{\mathrm{d}r}K_L(r) = -\frac{C}{r^2} \tag{3.18}$$

and we recognize equations (3.15) - (3.16) as the special form of the Bessel differential discussed in Appendix A, where we found (A.27) and (A.18) to be a solution to (3.15) and (3.16), respectively. For the complex Helmholtz equation we get

$$K_{cH_\pm}(r) = C\frac{e^{\pm\mu r}}{r} \tag{3.19}$$

$$\frac{\mathrm{d}}{\mathrm{d}r}K_{cH_\pm}'(r) = -C\left(\frac{1}{r} \mp \mu\right)\frac{e^{\pm\mu r}}{r} \tag{3.20}$$

We see that K_{cH_+} does not vanish at infinity, condition (3.13). This permits us to only consider K_{cH_-}, and to drop the ± notation. For the Helmholtz equation, we get

$$K_{H_\pm}(r) = C\frac{e^{\pm i\mu r}}{r} \tag{3.21}$$

$$\frac{\mathrm{d}}{\mathrm{d}r}K'_{H_\pm}(r) = -C\left(\frac{1}{r} \mp i\mu\right)\frac{e^{\pm i\mu r}}{r} \tag{3.22}$$

Now if we insert this into the identity (3.3), and because of the singularity at $r = 0$ we cut out from Ω a ball $B(\mathbf{y}, \rho)$ contained in Ω with center $\mathbf{y}$, radius ρ, and boundary $S(\mathbf{y}, \rho)$. The remaining region $\Omega_p = \Omega - B(\mathbf{y}, \rho)$. Since $\mathcal{L}'v = \mathcal{L}'K = 0$ in Ω_p we have

$$\int_{\Omega_p} \mathcal{L}'u \,\mathrm{d}x = \int_{\partial\Omega}\left(v\frac{\mathrm{d}u}{\mathrm{d}\mathbf{n}} - u\frac{\mathrm{d}v}{\mathrm{d}\mathbf{n}}\right)\mathrm{d}S + \int_{S(\mathbf{y},\rho)}\left(v\frac{\mathrm{d}u}{\mathrm{d}\mathbf{n}} - u\frac{\mathrm{d}v}{\mathrm{d}\mathbf{n}}\right)\mathrm{d}S \tag{3.23}$$

Here on $S(\mathbf{y}, \rho)$ the *exterior* normal to our region Ω_p points towards $\mathbf{y}$. Consequently

$$v = K(\rho) \tag{3.24}$$

$$\frac{\mathrm{d}v}{\mathrm{d}\mathbf{n}} = -K'(\rho) \tag{3.25}$$

hence,

$$\int_{S(\mathbf{y},\rho)} v\frac{\mathrm{d}u}{\mathrm{d}\mathbf{n}}\,\mathrm{d}S = K(\rho)\int_{S(\mathbf{y},\rho)}\frac{\mathrm{d}u}{\mathrm{d}\mathbf{n}}\,\mathrm{d}S = -K(\rho)\int_{B(\mathbf{y},\rho)}\mathcal{L}'u\,\mathrm{d}\mathbf{x} \tag{3.26}$$

the last step in (3.26) is carried out by using (3.4)

$$\int_{S(\mathbf{y},\rho)} u\frac{\mathrm{d}v}{\mathrm{d}\mathbf{n}}\,\mathrm{d}S = -K'(\rho)\int_{S(\mathbf{y},\rho)} u\,\mathrm{d}S \tag{3.27}$$

Noting both u and $\mathcal{L}'u$ is continuous at $\mathbf{y}$, we consider what happens when ρ goes to zero. We begin with considering the right hand side of (3.26) for each of the cases, where we use that the integral of a *continuous* function over an infinitely small surface is equal to the function value in the point, times the area of the surface, and we get

$$\lim_{\rho\to 0}\left[-K(\rho)\int_{B(\mathbf{y},\rho)}\mathcal{L}'u\,\mathrm{d}\mathbf{x}\right] = \begin{cases}\lim\limits_{\rho\to 0}\left[-\dfrac{C}{\rho}\displaystyle\int_{B(\mathbf{y},\rho)}\mathcal{L}'u\,\mathrm{d}\mathbf{x}\right] = 0\\ \lim\limits_{\rho\to 0}\left[-C\dfrac{e^{-\mu\rho}}{\rho}\displaystyle\int_{B(\mathbf{y},\rho)}\mathcal{L}'u\,\mathrm{d}\mathbf{x}\right] = 0\\ \lim\limits_{\rho\to 0}\left[-C\dfrac{e^{\pm i\mu\rho}}{\rho}\displaystyle\int_{B(\mathbf{y},\rho)}\mathcal{L}'u\,\mathrm{d}\mathbf{x}\right] = 0\end{cases} \tag{3.28}$$

and for (3.27) we use how the integral of a *continuous* function over an infinitely small volume is equal to the function value at the point, times the area, and we get

$$\lim_{\rho\to 0}\left[-K'(\rho)\int_{S(\mathbf{y},\rho)}u\,\mathrm{d}S\right] = \begin{cases}\lim\limits_{\rho\to 0}\left[\dfrac{C}{\rho^2}\displaystyle\int_{S(\mathbf{y},\rho)}u\,\mathrm{d}s\right] = u(\mathbf{y})4\pi C\\ \lim\limits_{\rho\to 0}\left[C\left(\dfrac{1}{\rho}+\mu\right)\dfrac{e^{-\mu\rho}}{\rho}\displaystyle\int_{S(\mathbf{y},\rho)}u\,\mathrm{d}S\right] = u(\mathbf{y})4\pi C\\ \lim\limits_{\rho\to 0}\left[C\left(\mp i\mu+\dfrac{1}{\rho}\right)\dfrac{e^{\pm i\mu\rho}}{\rho}\displaystyle\int_{S(\mathbf{y},\rho)}u\,\mathrm{d}S\right] = u(\mathbf{y})4\pi C\end{cases} \tag{3.29}$$

We have now found that equation (3.23) becomes

$$\int_\Omega v\mathcal{L}'u\,\mathrm{d}\mathbf{x} = \int_{\partial\Omega}\left(v\frac{\mathrm{d}u}{\mathrm{d}n}-u\frac{\mathrm{d}v}{\mathrm{d}n}\right)\mathrm{d}S - 4\pi C u(\mathbf{y}) \tag{3.30}$$

as ρ goes to zero.

Now if we choose $C = \frac{1}{4\pi}$, then $K(r)$ takes the form

$$K_L(r) = \frac{1}{4\pi r} \tag{3.31}$$

$$K_{cH}(r) = \frac{e^{-\mu r}}{4\pi r} \tag{3.32}$$

$$K_{H_\pm}(r) = \frac{e^{\pm i\mu r}}{4\pi r} \tag{3.33}$$

Next write the corresponding dependence on $\mathbf{x}$ and $\mathbf{y}$ as

$$v = K(\mathbf{x}, \mathbf{y}) = K(r) = K(|\mathbf{x} - \mathbf{y}|) \tag{3.34}$$

Then (3.30) becomes

$$u(\mathbf{y}) = \int_\Omega K(\mathbf{x}, \mathbf{y})(-\mathcal{L}')u \, \mathrm{d}\mathbf{x} + \int_{\partial\Omega} \left(K(\mathbf{x}, \mathbf{y}) \frac{\mathrm{d}u(\mathbf{x})}{\mathrm{d}n_\mathbf{x}} - u(\mathbf{x}) \frac{\mathrm{d}K(\mathbf{x}, \mathbf{y})}{\mathrm{d}n_\mathbf{x}} \right) \mathrm{d}S_\mathbf{x} \tag{3.35}$$

for $\mathbf{y} \in \Omega$, where the subscript $\mathbf{x}$ in $S_\mathbf{x}$ and $d\mathbf{n}_\mathbf{x}$ indicates the variable of integration and differentiation, respectively.

Since both $u(\mathbf{x})$ and $K(\mathbf{x}, \mathbf{y})$ vanish at $\partial\Omega$ (see equation (3.6)), the last term in equation (3.35) vanish, giving us

$$u(\mathbf{y}) = \int_{\Omega} K(\mathbf{x}, \mathbf{y})(-\mathcal{L}')u \, \mathrm{d}\mathbf{x} \tag{3.36}$$

now defining the operator $\mathcal{L}$

$$\mathcal{L} \stackrel{\text{def}}{=} -\mathcal{L}' \tag{3.37}$$

equation (3.36) takes the form

$$u(\mathbf{y}) = \int_{\Omega} K(\mathbf{x}, \mathbf{y})\mathcal{L}u \, \mathrm{d}\mathbf{x} \tag{3.38}$$

We look at (3.38) for a test function $\phi \in C_0^{\infty}(\Omega)$ then by integration by parts we find

$$\phi(\mathbf{y}) = \int K(\mathbf{x}, \mathbf{y})\mathcal{L}\phi(\mathbf{x}) \, \mathrm{d}\mathbf{x} = \int (\mathcal{L}K(\mathbf{x}, \mathbf{y}))\phi(\mathbf{x}) \, \mathrm{d}\mathbf{x} \tag{3.39}$$

meaning $\mathcal{L}K(\mathbf{x}, \mathbf{y})$ defines a distribution for which

$$\mathcal{L}K[\phi] = \phi(\mathbf{y}) \tag{3.40}$$

or put in other words $\mathcal{L}K(\mathbf{x}, \mathbf{y})$ defines the Dirac delta function with singularity at $\mathbf{y}$.

$$\mathcal{L}K(\mathbf{x}, \mathbf{y}) \stackrel{\text{def}}{=} \delta_{\mathbf{y}}(\mathbf{x}) \tag{3.41}$$

3.3 Fundamental solution to the Poisson, complex Helmholtz and Helmholtz equation

The problem we need the fundamental solution for in this thesis is the inhomogeneous Laplace equation (henceforth referred to as the Poisson equation), complex Helmhotz and the Helmholtz equation. In this section will we see how $K(\mathbf{x}, \mathbf{y})$ is a fundamental solution to these equations.

Consider

$$\mathcal{L}u(\mathbf{x}) = \rho(\mathbf{x}) \tag{3.42}$$

$$u(\mathbf{x}) = 0 \text{ on } \partial\Omega \tag{3.43}$$

Here we check if

$$u(\mathbf{y}) = \int K(\mathbf{x}, \mathbf{y})\rho(\mathbf{x})\, \mathrm{d}\mathbf{x} \tag{3.44}$$

is a solution to the system (3.42) - (3.43).

We do this by applying the operator $\mathcal{L}_\mathbf{y}$ taken with respect to $\mathbf{y}$ on (3.44).

$$\mathcal{L}_\mathbf{y} u(\mathbf{y}) = \mathcal{L}_\mathbf{y} \int K(\mathbf{x}, \mathbf{y})\rho(\mathbf{x})\, \mathrm{d}\mathbf{x} \tag{3.45}$$

$$= \int \mathcal{L}_\mathbf{y} K(|\mathbf{x} - \mathbf{y}|)\rho(\mathbf{x})\, \mathrm{d}\mathbf{x} \tag{3.46}$$

$$= \int (\mathcal{L}_\mathbf{x} K(|\mathbf{y} - \mathbf{x}|))\rho(\mathbf{x})\, \mathrm{d}\mathbf{x} \tag{3.47}$$

$$= \int \delta_\mathbf{y}(\mathbf{x})\rho(\mathbf{x})\, \mathrm{d}\mathbf{x} = u(\mathbf{y}) \tag{3.48}$$

which implies (3.44) is a solution. Thus $K(\mathbf{x}, \mathbf{y})$ as found in (3.31), (3.32) and (3.33) is fundamental solutions to the Poisson, complex Helmholtz and Helmholtz equation.

3.3.1 Sommerfeld radiation condition

We still have the ± notation for the fundamental solution of the Helmholtz equation. We get a unique solution by applying the Sommerfeld radiation condition [8]. Which in short states that sources of energy cannot be sinks absorbing energy. It is given symbolically as

$$\lim_{r\to\infty} r\left(\frac{\mathrm{d}K(r)}{\mathrm{d}r} - i\mu K(r)\right) = 0 \tag{3.49}$$

imposing this on $K_{H_\pm}$

$$\lim_{r\to\infty} r\left(\frac{\mathrm{d}K_{H_+}}{\mathrm{d}r} - i\mu K_{H_+}\right) = \lim_{r\to\infty} \frac{1}{4\pi}\left(i\mu - i\mu - \frac{1}{r}\right)e^{i\mu r} = 0 \tag{3.50}$$

and

$$\lim_{r\to\infty} r\left(\frac{\mathrm{d}K_{H_-}}{\mathrm{d}r} - i\mu K_{H_-}\right) = \lim_{r\to\infty} \frac{1}{4\pi}\left(-2i\mu - \frac{1}{r}\right)e^{-i\mu r} = -\frac{i}{2\pi}\mu \tag{3.51}$$

from this we see that K_{H-} does not satisfy the Sommerfeld condition, excluding it as a fundamental solution. Now since K_{H+} is the only solution of interest, we drop the ± notation.

3.4 Summary

Now let us write $P = K_L$, $H_c^\mu = K_{cH}$ and $H^\mu = K_H$. Then set $\Omega = \mathrm{R}^3$. We then have the free space kernels

$$P(r) = \frac{1}{4\pi r} \tag{3.52}$$

$$H_c^{\mu}(r) = \frac{e^{-\mu r}}{4\pi r} \tag{3.53}$$

$$H^{\mu}(r) = \frac{e^{i\mu r}}{4\pi r} \tag{3.54}$$

These will in the rest of the thesis be used to measure the accuracy of our approixmations to the free-space Poisson, complex Helmholtz and Helmholtz kernels.

4

Separable representations of the Poisson and complex Helmholtz kernels

In chapter 2 did we see how the complexity of applying an operator kernel $K(\mathbf{x}, \mathbf{y})$ in d dimensions went from $O((k+1)^{2d})$ to $O(dM(k+1)^{d+1})$, where k is the polynomial order of the basis, d is the dimension and M is the separation rank of the operator.

We begin the chapter by writing the free space Poisson and complex Helmholtz kernels in terms of integrals with separable superexponentially decaying integrands. The advantages of these forms are that the integrand dies superexponentially at both ends of the quadrature range so the equispaced quadrature range converges geometrically, and the required resolution is only weakly dependent on r.

We will then propose an algorithm designed to find the optimal quadrature range for integrating integrands that decay superexponentially. We then compare our results for the quadrature range of the schemes used in MRChem [9] for the Poisson and complex Helmholtz kernel.

4.1 Separable form of the Poisson kernel

In this section we go through the steps involved in expressing the three-dimensional Poisson kernel in terms of an integral over a superexponentially decaying Gaussian integrand. This form was first presented in [11] and was later used in [9], where its effective and accurate nature is displayed.

We begin by considering the problem

$$-\nabla^2 P(\mathbf{x}) = \delta_{\mathbf{y}}(\mathbf{x}) \tag{4.1}$$

$$P(\mathbf{x}) = 0 \text{ on } \partial\Omega \tag{4.2}$$

Next, on taking the Fourier transform of (4.1) we get

$$\mathbf{k}^2 \hat{P}(\mathbf{k}) = 1 \tag{4.3}$$

where

$$|\mathbf{k}| = \left(\sum_{i=1}^{3} k_i^2 \right)^{1/2} \tag{4.4}$$

Now if we divide the equation by $\mathbf{k}^2$ we see that $\hat{P}(\mathbf{k})$ can be written in terms of the integral

$$\hat{P}(\mathbf{k}) = \frac{1}{\mathbf{k}^2} = \int_0^\infty e^{-\mathbf{k}^2 \tau} \, \mathrm{d}\tau \tag{4.5}$$

Taking the inverse Fourier transform of (4.5) using $\mathcal{F}^{-1}[e^{-k_i^2 \tau}] = \frac{e^{-\frac{x_i^2}{4\tau}}}{2\sqrt{\pi\tau}}$, we find that the Poisson kernel can be written in terms of the integral

$$P(\mathbf{x}) = \frac{1}{8\pi^{3/2}} \int_{0^+}^\infty \frac{e^{-\frac{r^2}{4\tau}}}{\tau^{3/2}} \, \mathrm{d}\tau \tag{4.6}$$

where $r = \left(\sum_{i=1}^{3}(x_i - y_i)^2\right)^{1/2}$. Following this we write $P(r) = P(\mathbf{x})$. Now if we choose $\tau = \frac{1}{8t^2}$, the integral takes the form

$$P(r) = \frac{1}{\pi^{3/2}} \int_0^\infty e^{-4r^2t^2}\,\mathrm{d}t \tag{4.7}$$

We are now at the starting point of the derivation in [11, 9]. We continue with the substitution $t = \log(1 + e^u) - u$ and notice the limits

$$\lim_{u\to\infty} \log(1 + e^u) - u = \lim_{u\to\infty} \log(\exp[\log(1 + e^u) - u]) \tag{4.8}$$

$$= \lim_{u\to\infty} \log\left(1 + e^{-u}\right) = 0 \tag{4.9}$$

and

$$\lim_{u\to-\infty} \log(1 + e^u) - u = \infty \tag{4.10}$$

Equation (4.7) then takes the form

$$P(r) = \frac{1}{\pi^{3/2}} \int_{-\infty}^\infty \frac{e^{-4r^2(\log(1+e^u)-u)^2}}{1 + e^u}\,\mathrm{d}u \tag{4.11}$$

Finally, we substitute $u = -\sinh(w)$, obtaining the form

$$P(r) = \frac{1}{\pi^{3/2}} \int_{-\infty}^\infty \frac{\cosh(w)}{1 + e^{-\sinh(w)}} e^{-4r^2(\log\left(1+e^{-\sinh(w)}\right)+\sinh(w))^2}\,\mathrm{d}w \tag{4.12}$$

yielding superexponential decay of the integrand as w goes to plus and minus infinity

$$\frac{e^{2r^2}}{2\pi^{3/2}} e^{w-r^2e^{2w}} \text{ for } w \to \infty \tag{4.13}$$

$$\frac{e^{2r^2}}{2\pi^{3/2}} e^{-w-\frac{1}{2}e^{-w}} \text{ for } w \to -\infty \tag{4.14}$$

4.2 Separable form of the complex Helmholtz kernel

In this section we go through the steps involved in expressing the complex Helmholtz kernel in the Gaussian form found in [10]. Starting from the

differential form

$$-\left(\nabla^2 - \mu^2\right) H_c(\mathbf{x}) = \delta_{\mathbf{y}}(\mathbf{x}) \tag{4.15}$$

$$H_c(\mathbf{x}) = 0 \text{ on } \partial\Omega \tag{4.16}$$

we take the Fourier transform of eq. (4.15)

$$\left(\mathbf{k}^2 + \mu^2\right) \hat{H}_c(\mathbf{k}) = 1 \tag{4.17}$$

where

$$|\mathbf{k}| = \left(\sum_{i=1}^{3} k_i^2\right)^{1/2} \tag{4.18}$$

If we further divide equation (4.17) by $\mathbf{k}^2 + \mu^2$ we see that $\hat{H}_c(\mathbf{k})$ can be written in terms of the integral

$$\hat{H}_c(\mathbf{k}) = \frac{1}{\mathbf{k}^2 + \mu^2} = \int_0^\infty e^{-\left(\mathbf{k}^2+\mu^2\right)\tau} \, \mathrm{d}\tau \tag{4.19}$$

Now taking the inverse Fourier transform of (4.19) using $\mathcal{F}^{-1}[e^{-k_i^2\tau}] = \frac{e^{-\frac{x_i^2}{4\tau}}}{2\sqrt{\pi\tau}}$, we find

$$H_c(\mathbf{x}) = \frac{1}{8\pi^{3/2}} \int_{0^+}^\infty \frac{e^{-\frac{r^2}{4\tau}-\mu^2\tau}}{\tau^{3/2}} \, \mathrm{d}\tau \tag{4.20}$$

where $r = \left(\sum_{i=1}^{3}(x_i - y_i)^2\right)^{1/2}$. Following this we write $H_c(r) = H_c(\mathbf{x})$.

$$H_c(r) = \frac{1}{8\pi^{3/2}} \int_{0^+}^\infty \frac{e^{-\frac{r^2}{4\tau}-\mu^2\tau}}{\tau^{3/2}} \, \mathrm{d}\tau \tag{4.21}$$

Now if we choose $\tau = \frac{1}{4t^2}$ the integral takes the form

$$H_c(r) = \frac{1}{2\pi^{3/2}} \int_{0^+}^\infty e^{-r^2t^2-\frac{\mu^2}{4t^2}} \, \mathrm{d}t \tag{4.22}$$

Finally, we get the form presented in [10] through the substitution $t = e^{2w}$

$$\frac{1}{2\pi^{3/2}} \int_{-\infty}^\infty e^{-r^2e^{2w}-\frac{\mu^2}{4}e^{-2w}+w} \, \mathrm{d}w \tag{4.23}$$

Yielding superexponential decay of the integrand as w goes to plus and minus infinity

$$2\pi^{3/2} e^{-r^2 e^{2w} + w} \text{ for } w \to \infty \tag{4.24}$$

$$2\pi^{3/2} e^{-\frac{\mu^2}{4} e^{-2w} + w} \text{ for } w \to -\infty \tag{4.25}$$

4.3 Truncation error of integrals with superexponentially decaying integrands

Frediani [9] and Harrison [10] evaluates the integrals (4.12) and (4.44) by an equispaced quadrature rule[1]

$$\int_{-\infty}^{\infty} f(w)\,\mathrm{d}w \approx h \sum_{k=-\infty}^{\infty} f(w_k) \tag{4.26}$$

which in turn is truncated as

$$h \sum_{k=-\infty}^{\infty} f(w_k) \approx h \sum_{k=1}^{M} f(w_k) \tag{4.27}$$

In this section we present a method that gives crude estimates to the residues R due to the truncation of the infinite sum (4.27)

Consider the integral

$$\int_{-\infty}^{\infty} f(w)\,\mathrm{d}w \tag{4.28}$$

where $f(w)$ is a superexponentially decaying integrand. We evaluate this integral by the sum

$$h \sum_{k=-\infty}^{\infty} f(w_k) \approx h \sum_{k=1}^{M} f(w_k) \tag{4.29}$$

1. An equispaced quadrature means a constant step-size between each point evaluated, $w_{i+1} = w_i + h$.

To estimate the truncation errors

$$R_{upper} = h \sum_{k=M+1}^{\infty} f(w_k) \tag{4.30}$$

$$R_{lower} = h \sum_{k=-\infty}^{0} f(w_k) \tag{4.31}$$

we consider the ratios

$$v_{upper} = \frac{f(w_{M+1})}{f(w_{M+2})} \tag{4.32}$$

$$v_{lower} = \frac{f(w_{-2})}{f(w_{-1})} \tag{4.33}$$

Since $f(w)$ decays superexponentially, these ratios will decrease exponentially as w increases and decreases, respectively. Then by the sum for an infinite geometric series can we find an upper bound to the truncation error as

$$R_{upper} < \delta_{upper} = \left| \frac{hf(w_{M+1})}{1 - v_{upper}} \right| \tag{4.34}$$

$$R_{lower} < \delta_{lower} = \left| \frac{hf(w_{-1})}{1 - v_{lower}} \right| \tag{4.35}$$

Since the ratios v decay exponentially this is a rather crude estimate for the upper bound. However, as we will see, these estimates prove effective when we attempt to determine w_1 and w_M in the discretization of the integrals for the Poisson (4.12) and complex Helmholtz (4.44) kernels.

4.4 Numerical experiments with the Poisson kernel

In this section we approximate the Poisson kernel in the area $r \in [r_{min}, r_{max}]$ for a given error bound ϵ_s. Using the estimates for the truncation error displayed in 4.3 we develop algorithms designed to find an optimal separation rank M (algorithms 1 and 2), by the equispaced quadrature used in [9]. We then compare our results with the well established algorithm used in MRChem (algorithms 3 and 4).

4.4.1 New algorithms for limits of integration

We aim to approximate the Poisson kernel in the area $r \in [r_{min}, r_{max}]$. We begin by rescaling into the area $r' \in \left[r'_0, 1\right]$ where $r'_0 = \frac{r_{min}}{r_{max}}$, and reintroduce the Poisson kernel in its integral form

$$P(r') = \frac{1}{\pi^{3/2}} \int_{-\infty}^{\infty} \frac{\cosh(w)}{1 + e^{-\sinh(w)}} e^{-4r'^2(\log\left(1+e^{-\sinh(w)}\right)+\sinh(w))^2} \, \mathrm{d}w \tag{4.36}$$

where the integrand takes the asymptotic forms

$$\frac{e^{2r'^2}}{2\pi^{3/2}} e^{w-r'^2e^{2w}} \text{ for } w \to \infty \tag{4.37}$$

$$\frac{e^{2r'^2}}{2\pi^{3/2}} e^{-w-\frac{1}{2}e^{-w}} \text{ for } w \to -\infty \tag{4.38}$$

To determine the upper limit of integration w_M, we see that the superexponential decay in (4.37) is the least prominent for the smallest value of r', namely r'_0.

$$\frac{e^{2r_0'^2}}{2\pi^{3/2}} e^{w-r_0'^2e^{2w}} \geq \frac{e^{2r'^2}}{2\pi^{3/2}} e^{w-r'^2e^{2w}} \tag{4.39}$$

so to select the upper limit w_M for all $r' \in \left[r'_0, 1\right]$, we do it for $r' = r'_0$ and it will hold for all r'. To compute it we start with some guess for the value w_M, then increase it until we have a sufficiently small estimate δ_{upper} of the residue (4.35). We determine δ_{upper} empirically as

$$\delta_{upper} = \begin{cases} \frac{10^4}{4\pi r'_0}\epsilon_s \text{ for } \epsilon_s \leq 10^{-5} \\ \frac{10^2}{4\pi r'_0}\epsilon_s \text{ for } \epsilon_s > 10^{-5} \end{cases} \tag{4.40}$$

The procedure is displayed in the following algorithm.

Algorithm 1 Determination of upper limit of integration for (4.11) as discussed in this thesis

procedure $UpperLimit(r_0, \delta, h)$
  $w_M = Re(\log\left(\frac{-\log(\delta)}{r_0'^2}\right)/2)/2$
  $i = 0$
  while $\frac{exp(-r_0^2 e^{2(w_0+(i+1)h)}+(w_0+(i+1)h))}{(1-\frac{\exp\left(-r_0^2 e^{2(w_0+(i+2)h)}+(w_0+(i+2)h)\right)}{\exp\left(-r_0^2 e^{2(w_0+(i+1)h)}+(w_0+(i+1)h)\right)}} > \pm\delta$ **do**
    $i = i + 1$
  end while
  $w_M = w_M + ih$
  return w_M
end procedure

Similarly for w_0 we look at the integrand (4.38) and note that this has its largest value for $r' = 1$

$$\frac{e^2}{2\pi^{3/2}} e^{-w-\frac{1}{2}e^{-w}} \geq \frac{e^{2r^2}}{2\pi^{3/2}} e^{-w-\frac{1}{2}e^{-w}} \tag{4.41}$$

so to select the lower limit w_0 for all $r' \in [r_0, 1]$ it is sufficient to find it for $r' = 1$ and it will hold for all r'. To compute this we start with some guess for the value w_0, then decrease it until we have a sufficiently small estimate δ_{lower} of the residue (4.34). This is empirically determined to be

$$\delta_{lower} = \epsilon_s \tag{4.42}$$

The procedure is displayed in the following algorithm.

Algorithm 2 Determination of lower limit of integration for (4.11) as discussed in this thesis

procedure $LowerLimit(r_0, \delta, h)$
  $w_0 = w_M$
  $i = 0$
  while $w_0 > 0$ **do**
    $i = i + 1$
    $w_0 = w_0 - ih$
  end while
  while $\frac{\exp\left(-(w_0-(i+1)h)-\frac{1}{2}e^{-(w_0-(i+1)h)}\right)}{1-\frac{\exp\left(-(w_0-(i+2)h)-\frac{1}{2}e^{-(w_0-(i+2)h)}\right)}{\exp\left(-(w_0-(i+1)h)-\frac{1}{2}e^{-(w_0-(i+1)h)}\right)}} > \pm\delta$ **do**
    $i = i + 1$
  end while
  $w_0 = w_0 - ih$
  return w_0
end procedure

4.4.2 MRChem scheme for limits of integration

In the following algorithms we present the schemes for determining the lower and upper limits of integration as it is implemented in the MRChem program. The plan for creating this algorithm has been lost in time. The methods is presented here for benchmark reasons only. And are displayed in the following algorithms.

Algorithm 3 Determination of upper limit of integration for (4.11) as implemented in MRChem

procedure $UpperLimit(\epsilon_s, r_0)$
  $T = 1$
  while $\sqrt{T}e^{-T}/r_0 > \epsilon_s$ **do**
    $T = 1.1T$
  end while
  $w_M = \log(T/r_0^2)/2$
  return w_M
end procedure

Algorithm 4 Determination of lower limit of integration for (4.11) as implemented in MRChem

procedure $LowerLimit(\epsilon_s)$
  $T = 1$
  while $2Te^{-T} > \epsilon_s$ **do**
    $T = 1.1T$
  end while
  $w_0 = -\log(2T)$
  return w_0
end procedure

Remark. *It may be noted that the same separation rank is found if the ending condition for the lower limit is set as "integrand less than ϵ_s", and the upper limit is set as "integrand is less than $\epsilon_s \frac{1}{4\pi r_0'}$". In algorithms 1 and 2 respectfully.*

4.4.3 Results

For the numerical experimentation shown here. The area we are trying to find accurate representations are set to $|\mathbf{x}| \in [r_{min}, r_{max}]$. We fix set $r_{max} = \sqrt{3}$. This choice is motivated by the fact that we require expansions to be valid within the three-dimensional interval $[0, 1]^3$, thus the longest possible distance

between two points are $\sqrt{3}$. For the experiments shown here we use the step-size h presented in [10].

$$h = \frac{1}{0.2 - 0.47 \log_{10}(\epsilon_s)} \tag{4.43}$$

In Table 4.1 and in Figure 4.1 we see that there is not much to be gained from the new implementation of the Poisson kernel. The reason for this is simply that the original algorithm is already well optimized.

In Figures 4.2 and 4.3 we see examples of the relative pointwise error $e_{\epsilon_s,r}$, for the MRChem scheme and the new scheme presented here. When it comes to the spikes we see in Figures 4.2 and 4.3 for large r, where the error is not within the requested bounds, has been shown in the supplementary material of [9] not to influence the final precision of the result[2].

In Figure 4.4 do we outline the reason for the slight reduction in separation rank. While the old scheme overshoots a bit on the minimum threshold, we hit it perfectly.

r_{min}	ϵ_s	M_{old}	M_{new}	$difference$
1×10^{-4}	1×10^{-6}	47	44	3
1×10^{-4}	1×10^{-8}	62	60	2
1×10^{-4}	1×10^{-12}	94	91	3
1×10^{-6}	1×10^{-6}	61	58	3
1×10^{-6}	1×10^{-8}	81	78	3
1×10^{-6}	1×10^{-12}	121	119	2

Table 4.1: Separation rank for MRChem scheme (M_{old}) and thesis scheme (M_{new}), for the Poisson kernel. With corresponding difference $M_{old} - M_{new}$

2. Convolutions with the kernel

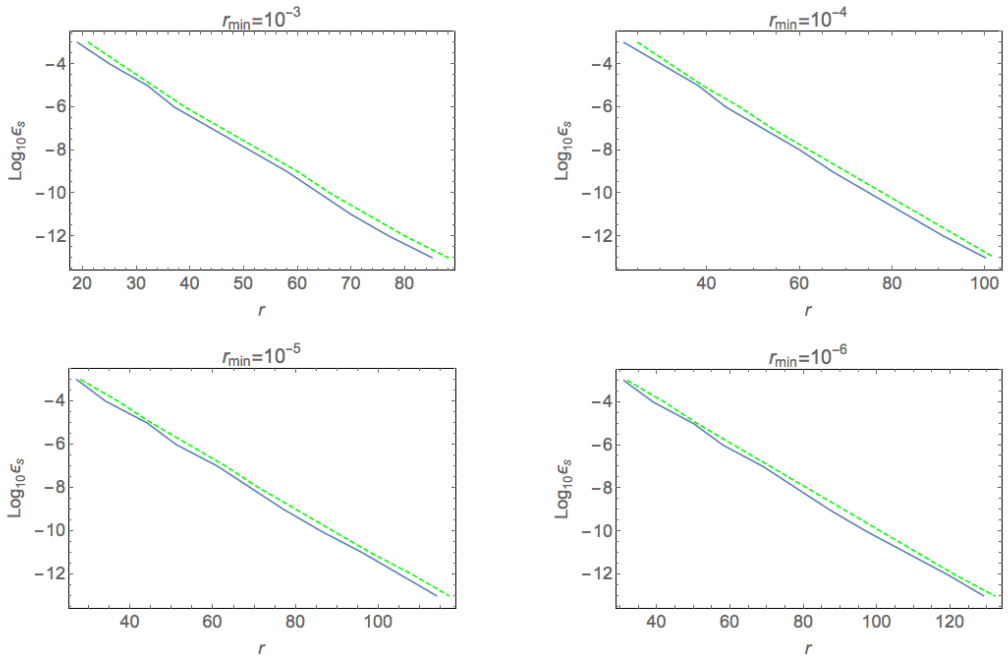

Figure 4.1: The $\log_{10}$ of ϵ_s versus separation rank for old (green dashed) and new (blue) approximation. For $r_{min} = 10^{-3}, 10^{-4}, 10^{-5}, 10^{-6}$.

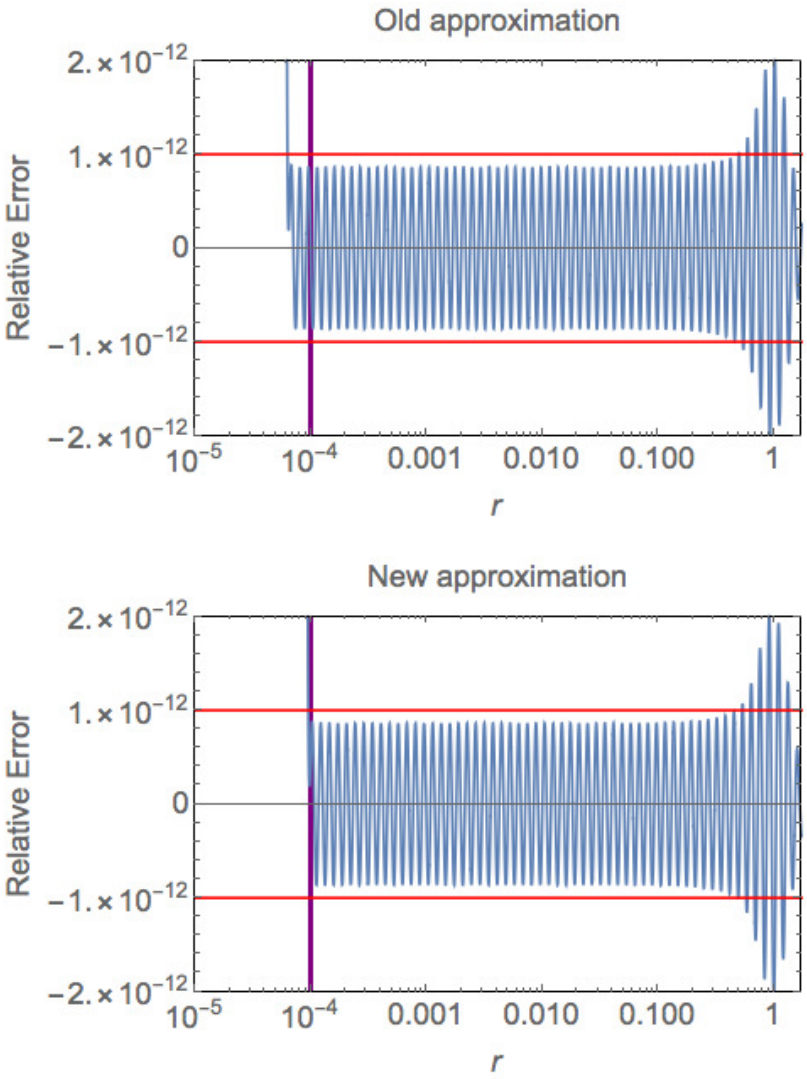

Figure 4.2: Old and new approximation: Plot of relative error $(P(r) - \hat{P}(r))/P(r)$ versus r. $r_{min} = 10^{-4}$, $r_{max} = \sqrt{3}$ and $\epsilon_s = 10^{-12}$. Error bound ϵ_s in red and minimum threshold r_{min} displayed in purple. With separation ranks $M_{old} = 94$ and $M_{new} = 91$.

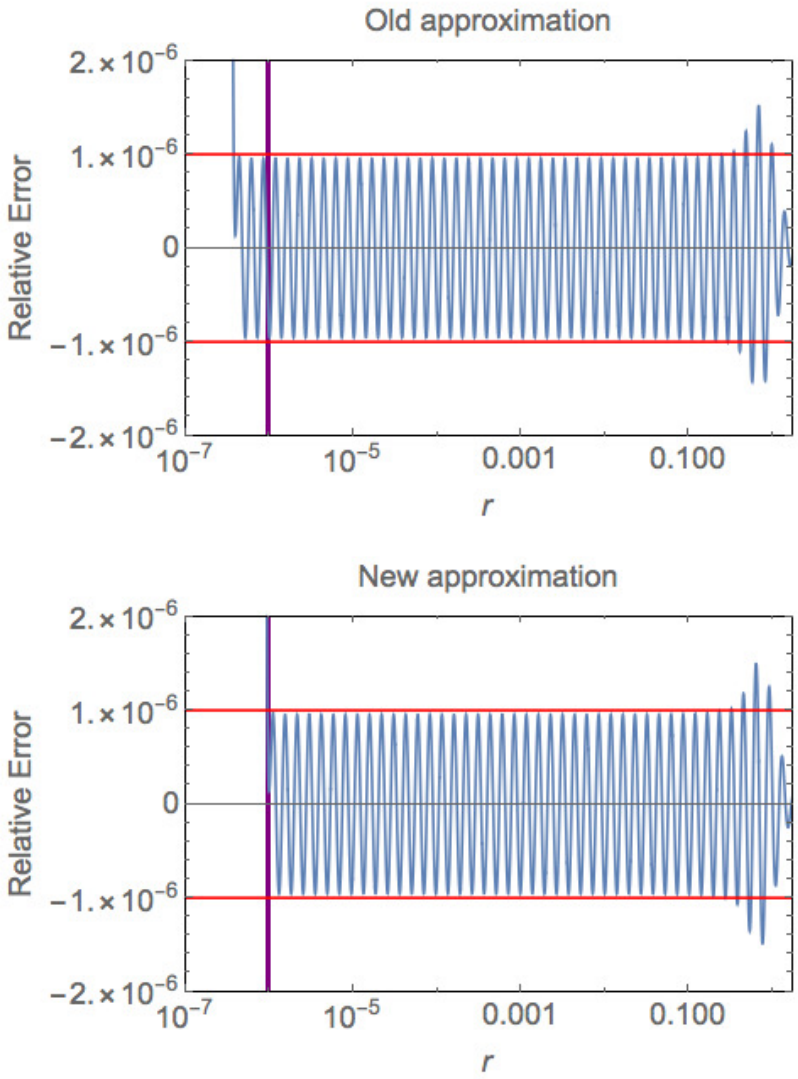

Figure 4.3: Old and new approximation: Plot of relative error $(P(r) - \hat{P}(r))/P(r)$ versus r. $r_{min} = 10^{-6}$, $r_{max} = \sqrt{3}$ and $\epsilon_s = 10^{-6}$. Error bound ϵ_s in red minimum threshold r_{min} displayed in purple. With separation ranks $M_{old} = 61$ and $M_{new} = 58$.

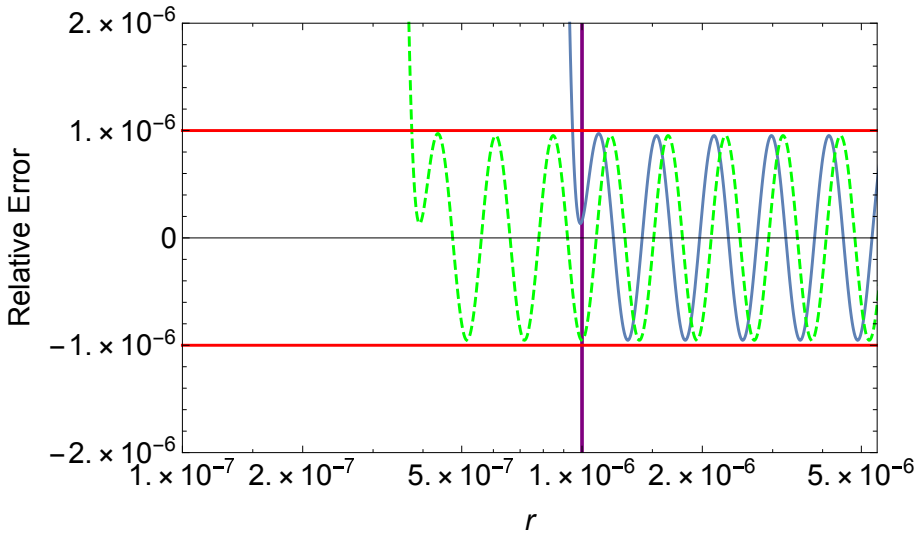

Figure 4.4: Zoomed in comparison of overshooting by old scheme (*green dashed*) and new scheme (*blue*) near the minimum threshold r_{min}. $r_{min} = 10^{-6}$, $r_{max} = \sqrt{3}$ and $\epsilon_s = 10^{-6}$

Remark. *Something of note, the equispaced quadrature used for these integrals are often in the literature referred to as trapezoidal quadrature. This often leads to a misunderstanding in the implementation of these kernels. As opposed to the equispaced quadrature where each discretization point is weighed by the step-size h, a trapezoidal rule weigh the first and last term in the series by half. For carefully chosen first and last terms as presented in this work, such a trapeziodal rule will result in missing the threshold mark.*

4.5 Numerical experiments with complex Helmholtz kernel

In this section we approximate the complex Helmholtz kernel in the area $r \in [r_{min}, r_{max}]$ for a given error bound ϵ_s. Using the estimates for the truncation error displayed in 4.3 we develop algorithms designed to find an optimal separation rank M (algorithms 5 and 6), by the equispaced quadrature used

in [10]. We then compare our results with the well established algorithm used in MRChem (algorithm 7).

4.5.1 New algorithms for limits of integration

We aim to approximate the complex Helmholtz kernel in the area $r \in [r_{min}, r_{max}]$. We begin by rescaling into the area $r' \in [r'_0, 1]$ where $r'_0 = \frac{r_{min}}{r_{max}}$, and reintroduce the complex Helmholtz kernel in its integral form

$$H_c(r') = \frac{1}{2\pi^{3/2}} \int_{-\infty}^{\infty} e^{-r'^2 e^{2w} - \frac{\mu'^2}{4} e^{-2w} + w} \, \mathrm{d}w \tag{4.44}$$

where the integrand takes the asymptotic form

$$2\pi^{3/2} e^{-r^2 e^{2w} + w} \text{ for } w \to \infty \tag{4.45}$$

$$2\pi^{3/2} e^{-\frac{\mu'^2}{4} e^{-2w} + w} \text{ for } w \to -\infty \tag{4.46}$$

with the rescaled $\mu' = \mu r_{max}$.

To determine the upper limit of integration w_M, we see that the superexponential decay in (4.45) is the least prominent for the smallest value of r', namely r_0

$$2\pi^{3/2} e^{-r'^2_0 e^{2w} + w} \geq 2\pi^{3/2} e^{-r'^2 e^{2w}} \tag{4.47}$$

So to select the upper limit w_M for all $r' \in [r'_0, 1]$ we do it for $r' = r'_0$ and it will hold for all r'. To compute it we start with some guess for the value w_M, then increase it until we have a sufficiently small estimate δ_{upper} of the residue (4.34). This is empirically determined to be

$$\delta_{upper} = \epsilon_s \frac{e^{-\mu' r'_0}}{4\pi r'_0} 10^4 \tag{4.48}$$

The procedure is displayed in the following algorithm.

Algorithm 5 Determination of upper limit of integration for (4.44) as discussed in this thesis

procedure $UpperLimit(\mu, \delta, h)$
  $w_M = Re(\log\left(\frac{-\log(\delta)}{r_0'^2}\right)/2)/2$
  $i = 0$
  while $\frac{\exp\left(-r_0^2 e^{2(w_0+(i+1)h)}+(w_0+(i+1)h)\right)}{(1-\frac{\exp\left(-r_0^2 e^{2(w_0+(i+2)h)}+(w_0+(i+2)h)\right)}{\exp\left(-r_0^2 e^{2(w_0+(i+1)h)}+(w_0+(i+1)h)\right)}} > \pm\delta$ **do**
    $i = i + 1$
  end while
  $w_M = w_M + ih$
  return w_M
end procedure

Similarly for w_0 we look at the integrand (4.46) and note that this is independent of r

$$\frac{e^2}{2\pi^{3/2}} e^{-\frac{-\mu'^2}{4}} e^{-2w+w} \tag{4.49}$$

so we just need to select w_0 such that this is small enough. We compute it by a using w_M as a starting guess, then integrate down with the step-size h,[3] until we have a sufficiently small estimate δ_{lower} of the residue (4.35). This is empirically determined to be

$$\delta_{lower} = \epsilon_s \tag{4.50}$$

The procedure is displayed in the following algorithm.

3. The reason for this odd way of iterating is simply that it will force the separation rank down.

Algorithm 6 Determination of lower limit of integration for (4.44) as discussed in this thesis

procedure $LowerLimit(r_0, \delta, h, w_M)$
  $w_0 = w_M$
  $i = 0$
  while $\frac{\exp\left(-\frac{\mu^2}{4}e^{-2(w_0-(i+1)h)}+(w_0-(i+1)h)\right)}{(1-\frac{\exp\left(-\frac{\mu^2}{4}e^{-2(w_0-(i+2)h)}+(w_0-(i+2)h)\right)}{\exp\left(\frac{\mu^2}{4}e^{2(w_0-(i+1)h)}+(w_0-(i+1)h)\right)}} > \pm\delta$ **do**
    $i = i + 1$
  end while
  $w_0 = w_0 - ih$
  return $w_{min} = w_0$
end procedure

4.5.2 MRChem for limits of integration

The upper and lower limits is for the complex Helmholtz kernel [10] are found to be

$$w_M = \frac{\log\left(\frac{T}{r_0'^2}\right)}{2} \tag{4.51}$$

$$w_0 = -\frac{\log\left(\frac{4T}{\mu'^2}\right)}{2} \tag{4.52}$$

$$\tag{4.53}$$

where $T = -2.5\log(\epsilon_s)$ is an empirically determined parameter. The procedure is displayed in the following algorithm.

Algorithm 7 Determination of upper and lower limit of integration for (4.44) as implemented in MRChem

procedure $UpperLimit(r_0, \epsilon_s)$
$T = -2.5 \log(\epsilon_s)$
$w_{min} = -0.5 \log \frac{4T}{\mu^2}$
$w_{max} = 0.5 \log \frac{T}{r_0^2}$
return w_{min} and w_{max}
end procedure

4.5.3 Results

For the numerical experimentation shown here. The area we are trying to find accurate representations are set to $|\mathbf{x}| \in [r_{min}, r_{max}]$. We fix set $r_{max} = \sqrt{3}$. This choice is motivated by the fact that we require expansions to be valid within the three-dimensional interval $[0, 1]^3$, thus the longest possible distance between two points are $\sqrt{3}$. For the experiments shown here we use the step-size h presented in [10].

$$h = \frac{1}{0.2 - 0.47 \log_{10}(\epsilon_s)} \tag{4.54}$$

In Table 4.2 and in Figures 4.5-4.6 we see that in this case there is more to be gained from new implementation of the complex Helmholtz kernel.

In Figures 4.7 and 4.8 we see examples of the relative pointwise error $e_{\epsilon_s,r}$, for the MRChem scheme and the new scheme presented here. In Figure 4.3 do we see how for large values of μ does the approximation run outside our requested bounds. In the supplementary material of [9] is it shown how this does not influence the final precision of the result.

In Figure 4.9 do we outline the reason for the slight reduction in separation rank. While the old scheme overshoots a bit on the minimum threshold, we

hit it perfectly.

r_{min}	ϵ_s	μ	M_{old}	M_{new}	$difference$
1×10^{-4}	1×10^{-6}	100	28	24	4
1×10^{-4}	1×10^{-6}	0.1	49	44	5
1×10^{-4}	1×10^{-8}	100	38	33	5
1×10^{-4}	1×10^{-8}	0.1	65	59	6
1×10^{-4}	1×10^{-12}	100	57	51	6
1×10^{-4}	1×10^{-12}	0.1	98	90	8
1×10^{-6}	1×10^{-6}	100	42	38	4
1×10^{-6}	1×10^{-6}	0.1	63	58	5
1×10^{-6}	1×10^{-8}	100	56	51	5
1×10^{-6}	1×10^{-8}	0.1	83	77	6
1×10^{-6}	1×10^{-12}	100	84	78	6
1×10^{-6}	1×10^{-12}	0.1	124	118	6

Table 4.2: Separation rank for MRChem scheme (M_{old}) and thesis scheme M_{new} for the complex Helmholtz kernel. With corresponding difference $M_{old} - M_{new}$

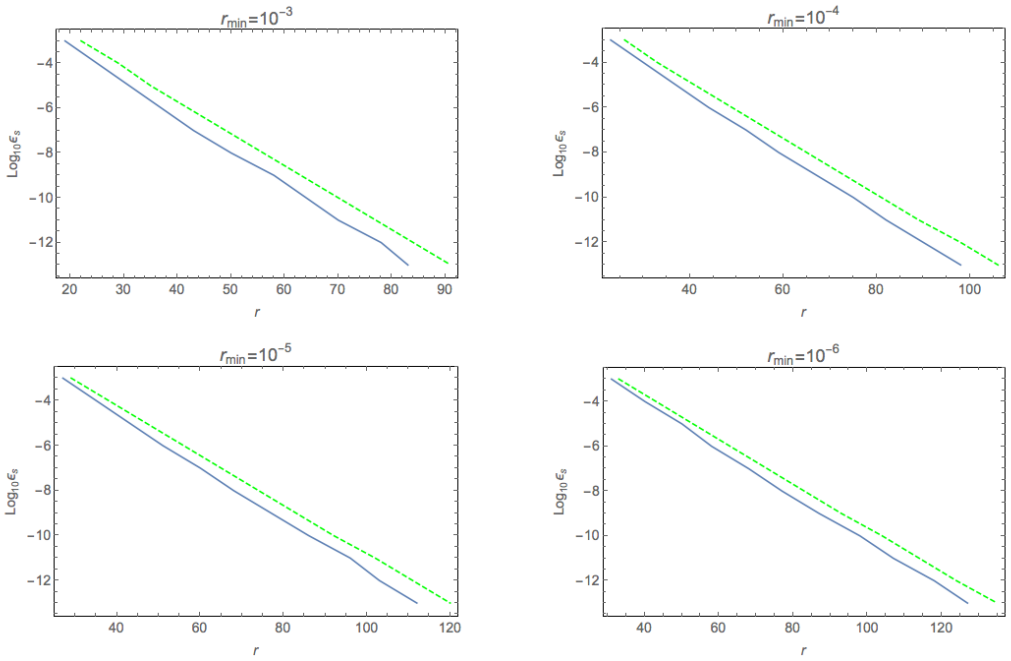

Figure 4.5: The $\log_{10}$ of ϵ_s versus separation rank for old (green dashed) and new (blue) approximation. For $\mu = 0.1$ $r_{min} = 10^{-3}, 10^{-4}, 10^{-5}, 10^{-6}$.

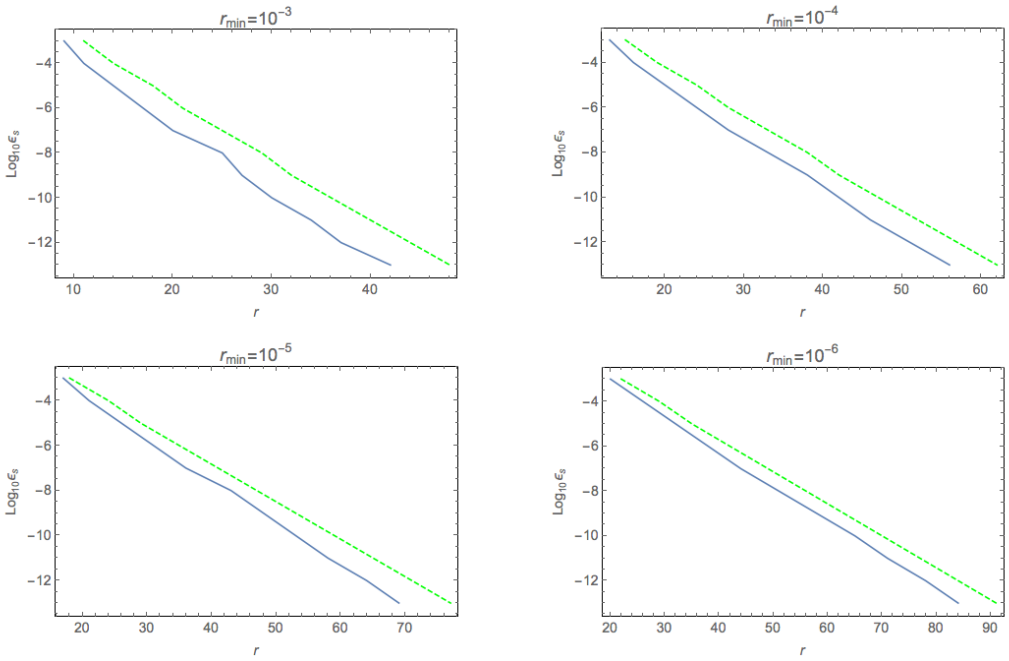

Figure 4.6: Complex Helmholtz: $\log_{10}$ of ϵ_s versus separation rank for old (green dashed) and new (blue) approximation. For $\mu = 100$ and $r_{min} = 10^{-3}, 10^{-4}, 10^{-5}, 10^{-6}$.

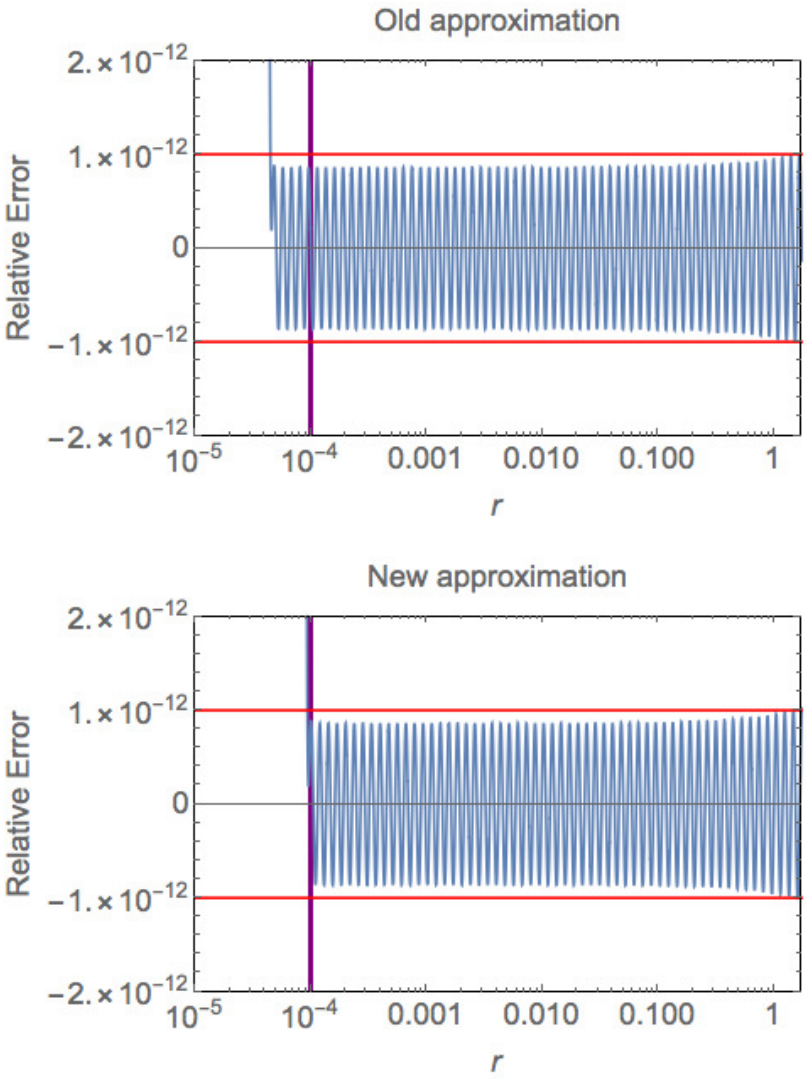

Figure 4.7: Old and new approximation: Plot of relative error $(H_c(r) - \tilde{H}_c(r))/H_c(r)$ versus r. $r_{min} = 10^{-4}, r_{max} = \sqrt{3}, \mu = 0.1$ and $\epsilon_s = 10^{-12}$. Error bound ϵ_s in red and minimum threshold r_{min} displayed in purple. With separation ranks $M_{old} = 98$ and $M_{new} = 90$

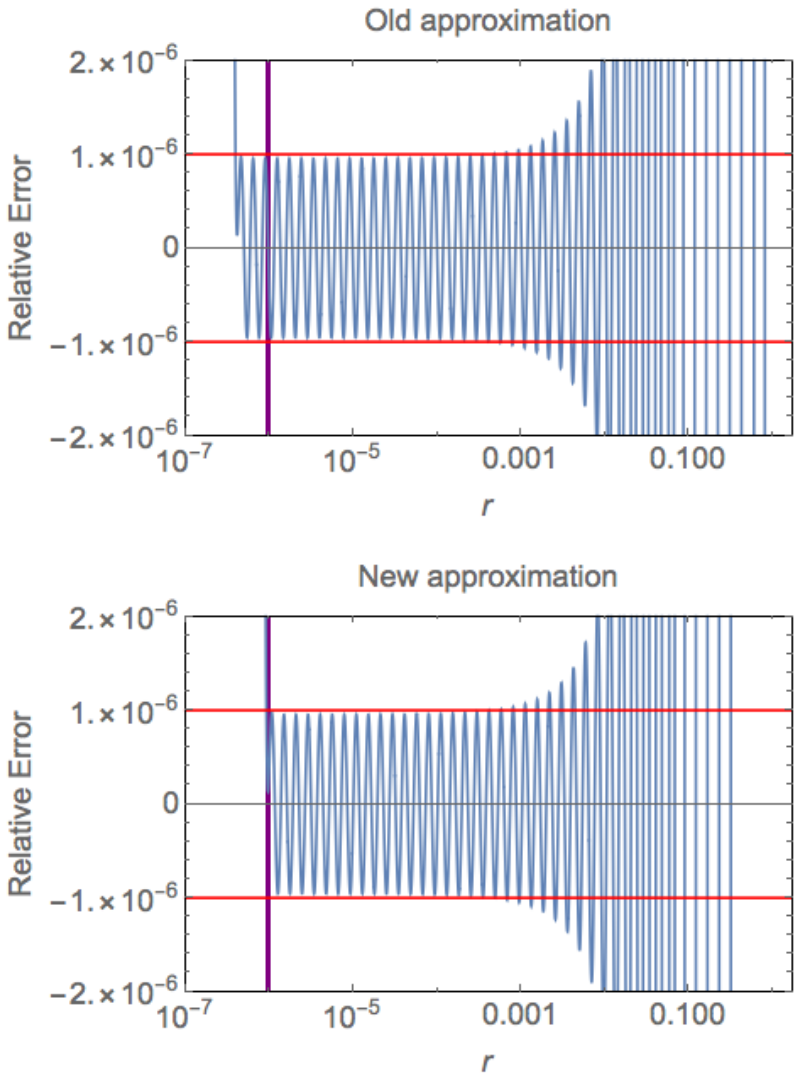

Figure 4.8: Old and new approximation: Plot of relative error $(H_c(r) - \tilde{H}_c(r))/H_c(r)$ versus r. $r_{min} = 10^{-6}, r_{max} = \sqrt{3}, \mu = 100$ and $\epsilon_s = 10^{-6}$. Error bound in red and minimum threshold (r_{min}) displayed in purple. With separation ranks $M_{old} = 42$ and $M_{new} = 38$

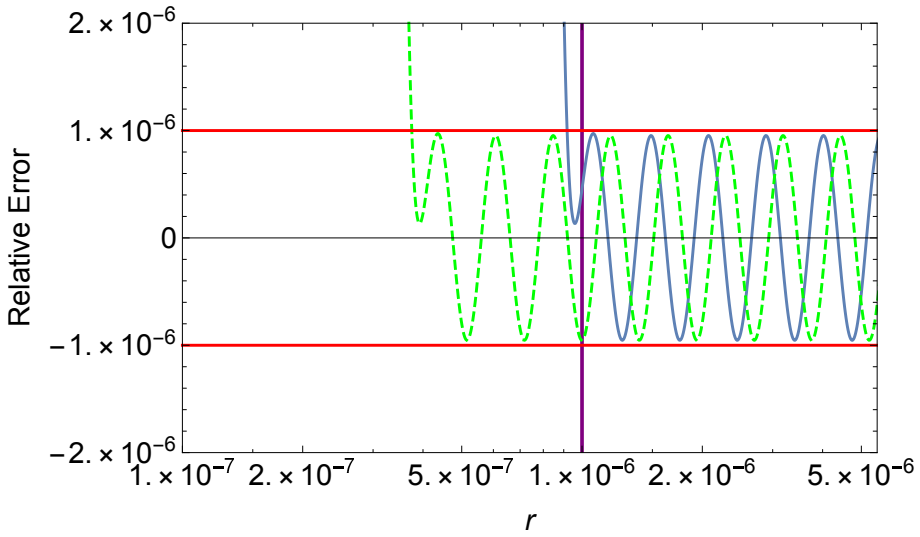

Figure 4.9: Zoomed in comparison of overshooting by old scheme (*green dashed*) and new scheme (*blue*) near the minimum threshold r_{min}. $r_{min} = 10^{-6}$, $r_{max} = \sqrt{3}$, $\mu = 100$ and $\epsilon_s = 10^{-6}$.

5

Approximation of the Helmholtz kernel

The goal with this chapter is to find a separable approximation to the free space Helmholtz kernel. We begin by following the approach used in chapter 4, where we found separable representations to the free space Poisson and complex Helmholtz kernels. Then we see where this approach fails in generating separable representations for the Helmholtz kernel. We then outline the approach by Beylkin [12] for fast convolutions with the Helmholtz kernel. This approach is inspired by the work of Ewald in [13]. Here Beylkin finds a way where parts of the free space Helmholtz kernel can be expressed in a separable form. However, convolutions with the remaining parts of the kernel has to be done by multiplications (of singular functions) in the Fourier domain. This can be done effectively and accurately by following the grid constructions described in [14, 15, 16]. In addition to this, these methods require an efficient implementation of the Non-Uniform Fast Fourier Transform

(NUFFT) [17, 18, 19].

Finally, we propose a new separable representation of the free space Helmholtz kernel, inspired by the work of Ewald in his doctoral thesis from 1912 [20].

Let us consider the problem

$$-\left(\nabla^2 + \mu^2\right) H(\mathbf{x}) = \delta_{\mathbf{y}}(\mathbf{x}) \tag{5.1}$$

$$H(\mathbf{x}) = 0 \text{ on } \partial\Omega \tag{5.2}$$

Next, we take the Fourier transform of (5.1)

$$\left(\mathbf{k}^2 - \mu^2\right) \hat{G}(\mathbf{k}) = 1 \tag{5.3}$$

where

$$|\mathbf{k}| = \left(\sum_{i=1}^{d} k_i^2 \right)^{1/2} \tag{5.4}$$

Now if we divide the equation by $\mathbf{k}^2 - \mu^2$, we get

$$\hat{G}(\mathbf{k}) = \frac{1}{\mathbf{k}^2 - \mu^2} \tag{5.5}$$

We see that we can no longer use the trick where we write $\frac{1}{\mathbf{k}^2-\mu^2} = \int_0^\infty e^{-(\mathbf{k}^2-\mu^2)\tau}\, \mathrm{d}\tau$, as the integral does not converge when $\mathbf{k}^2 < \mu^2$. So we need to come up with some other plan to find a suitable representation of the Helmholtz kernel. We will begin with discussing the approach by Beylkin [12].

5.1 Beylkin's approach

In [12] Beylkin shows how the Helmholtz kernel can be written in terms of the regularization

$$G(\mathbf{x}) = \lim_{\lambda \to 0^+} \frac{1}{(2\pi)^d} \int \frac{1}{|\mathbf{k}|^2 - (\mu - i\lambda)^2} \, \mathrm{d}\mathbf{k} \tag{5.6}$$

Next, let us define

$$\hat{G}(\kappa,\lambda) = \frac{1}{\kappa^2 - (\mu + i\lambda)^2} \tag{5.7}$$

where $\kappa = |k|$. We split this into its real and imaginary part

$$Re(\hat{G}(\kappa,\lambda)) = \frac{1}{2\kappa}\left(\frac{\kappa-\mu}{(\kappa-\mu)^2+\lambda^2} + \frac{\kappa+\mu}{(\kappa+\mu)^2+\lambda^2}\right) \tag{5.8}$$

and

$$Im(\hat{G}(\kappa,\lambda)) = \frac{1}{2\kappa}\left(\frac{\lambda}{(\kappa-\mu)^2+\lambda^2} - \frac{\lambda}{(\kappa+\mu)^2+\lambda^2}\right) \tag{5.9}$$

$$\tag{5.10}$$

On taking the limit, we get

$$\int_0^\infty \lim_{\lambda\to 0^+} Re(\hat{G}(\kappa,\lambda))\,\mathrm{d}\kappa = PV_{\kappa=\mu}\int_0^\infty \frac{1}{\kappa^2-\mu^2}\,\mathrm{d}\kappa \tag{5.11}$$

and

$$\int_0^\infty \lim_{\lambda\to 0^+} Im(\hat{G}(\kappa,\lambda))\,\mathrm{d}\kappa = \int_0^\infty \frac{\pi}{2\kappa}\left(\delta(\kappa-\mu) - \delta(\kappa+\mu)\right)\,\mathrm{d}\kappa \tag{5.12}$$

$$= \int_0^\infty \frac{\pi}{2\kappa}\delta(\kappa-\mu)\,\mathrm{d}\kappa \tag{5.13}$$

so we have

$$G(\mathbf{x}) = \frac{1}{(2\pi)^d} PV_{|\mathbf{k}|=\mu}\int \frac{e^{i\mathbf{x}\cdot\mathbf{k}}}{|\mathbf{k}|^2-\mu^2}\,\mathrm{d}\mathbf{k} + i\frac{\pi}{2(2\pi)^d}\int \frac{\delta(|\mathbf{k}|-\mu)}{|\mathbf{k}|}e^{-i\mathbf{x}\cdot\mathbf{k}}\,\mathrm{d}\mathbf{k} \tag{5.14}$$

Now we take a closer look at the imaginary part of $G(\mathbf{x})$ in (5.14)

$$Im(G(\mathbf{x})) = \frac{\pi}{2(2\pi)^d}\int \frac{\delta(|\mathbf{k}|-\mu)}{|\mathbf{k}|}e^{-i\mathbf{x}\cdot\mathbf{k}}\,\mathrm{d}\mathbf{k} \tag{5.15}$$

By the convolution theorem, (see e.g. [21]), convolutions in real space can be done as multiplications in Fourier space

$$[Im(G) * f](\mathbf{x}) = \frac{\pi}{2(2\pi)^d}\int \hat{f}(\mathbf{k})\frac{\delta(|\mathbf{k}|-\mu)}{|\mathbf{k}|}\mathbf{k}e^{-i\mathbf{x}\cdot\mathbf{k}}\,\mathrm{d}\mathbf{k} \tag{5.16}$$

which corresponds to an integral over a sphere.

Now let us take a closer look at the real part of $\hat{G}(\kappa, \lambda)$

$$\hat{G}(\kappa, \lambda) = \frac{1}{\kappa^2 - \mu^2} \tag{5.17}$$

We split this into two parts, a singular and an oscillatory part (as seen from real space)

$$\frac{1}{\kappa^2 - \mu^2} = \hat{F}_{sing}(\kappa) + \hat{F}_{oscill}(\kappa) \tag{5.18}$$

where

$$\hat{F}_{sing}(\kappa) = \frac{1 - e^{-\alpha^2(\kappa^2 - \mu^2)/\mu^2}}{\kappa^2 - \mu^2} \tag{5.19}$$

and

$$\hat{F}_{oscill}(\kappa) = \frac{e^{-\alpha^2(\kappa^2 - \mu^2)/\mu^2}}{\kappa^2 - \mu^2} \tag{5.20}$$

using the following parameters

$$\alpha^2 = \frac{\log \delta^{-1}}{b^2 - 1} \tag{5.21}$$

with $b > 1$. The purpose of these parameters will become clear shortly. Let us first invert $\hat{F}_{sing}$. We do this by using

$$\frac{1 - e^{-\alpha^2(\kappa - \mu^2)/\mu^2}}{\kappa^2 - \mu^2} = 2 \int_{-\infty}^{\log \frac{\alpha}{\mu}} e^{-r^2 \frac{e^{2s'}}{4} + \mu^2 e^{-2s'} + (d-2)s'} \, \mathrm{d}s' \tag{5.22}$$

then we use the inverse Fourier transform $\mathcal{F}^{-1}[e^{-k_i^2 e^{2s'}}] = \frac{e^{-\frac{x_i^2 e^{-2s'}}{4}} e^{-s'}}{2\sqrt{\pi}}$, and substitute $s' = -s$. $\hat{F}_{sing}$ is then found to be

$$F_{sing}(r) = \frac{1}{2^{d-1}\pi^{d/2}} \int_{-\log \frac{\alpha}{\mu}}^{\infty} e^{-r^2 \frac{e^{2s}}{4} + \mu^2 e^{-2s}} + (d-2)s \, \mathrm{d}s \tag{5.23}$$

F_{sing} can then be written as a sum of Gaussians. We now have a separable representation of the *singular* part of the Helmholtz kernel.

Similarly as for the imaginary part of the operator, we do the convolution with the oscillatory part of the real part as multiplications in Fourier space

$$[F_{oscill} * f](\mathbf{x}) = \frac{1}{(2\pi)^d} PV_{\mathbf{k}=\mu} \int \hat{F}_{oscill}(\mathbf{k}) \hat{f}(\mathbf{k}) e^{i\mathbf{x}\cdot\mathbf{k}} \, \mathrm{d}\mathbf{k} \tag{5.24}$$

And since $\alpha^2 = \frac{\log \delta^{-1}}{b^2 - 1}$, $\hat{F}_{oscill}$ is less than δ this can again be approximated by

$$[F_{oscill} * f](\mathbf{x}) \approx \frac{1}{(2\pi)^d} PV_{\mathbf{k}=\mu} \int_{|\mathbf{k}|<b\mu} \hat{F}_{oscill}(\mathbf{k}) \hat{f}(\mathbf{k}) e^{i\mathbf{x}\cdot\mathbf{k}} \, \mathrm{d}\mathbf{k} \tag{5.25}$$

The principal value is avoided in [12] by approximating $\hat{F}_{oscill}$ in the region $|\kappa - \mu| \geq min\{\mu\delta, \delta\}$ following the constructions in [15]. The integral is then transformed into spherical coordinates, where the angular quadrature points can be generated by following [14], and the grid points in radial direction is found by following [22]. The function $f(\mathbf{x})$ is transformed into the quadrature points in Fourier space by the non-uniform fast Fourier transform, see [17, 18, 19].

5.2 Separated representation of the Helmholtz kernel

In [20] Ewald shows how the Helmholtz kernel can be written in terms of the integral

$$H^{\mu}(r) = \frac{1}{2\pi^{3/2}} \int_{\Gamma} e^{-r^2 t^2 + \frac{\mu^2}{4t^2}} \, \mathrm{d}t \tag{5.26}$$

where Γ is an appropriately chosen contour. Later in [13] Ewald follows an approach similar to the one displayed in the previous section where instead of integrating along a contour in complex space, the integral is done in real space and the parameter μ is expanded to $\mu + i\lambda$. However, for those approaches the separability of the Helmholtz kernel is lost, but (5.26) inspires us to look for contours in the complex plane that yields fast convergent approximations to the Helmholtz kernel.

Inspired by this we found the integral

$$H^{\mu}(r) = \frac{1}{2\pi^{3/2}} \int_0^{\infty} e^{-r^2(\gamma i - t)^2 + \frac{\mu^2}{4(\gamma i - t)^2}} \, \mathrm{d}t - \frac{i}{2\pi^{3/2}} \int_0^{\gamma} e^{r^2 t^2 - \frac{\mu^2}{4t^2}} \, \mathrm{d}t \tag{5.27}$$

where $\gamma > 0$ which we in principle can select freely.

As an argument to show that these integrals compose the Helmholtz kernel can be done by the following argument: By using [23] we find that the integrals in (5.27) can be expressed in terms of error functions

$$\frac{1}{2\pi^{3/2}} \int_0^{\infty} e^{-r^2(\gamma i - t)^2 + \frac{\mu^2}{4(\gamma i - t)^2}} \, \mathrm{d}t = \tag{5.28}$$

$$\frac{e^{-i\mu r}}{8\pi r} \left[1 - e^{i2\mu r} \left(1 + \operatorname{erf}\left(\frac{\mu}{2\gamma} + ir\gamma \right) \right) + i \operatorname{erfi}\left(r\gamma + i\frac{\mu}{2\gamma} \right) \right] \tag{5.29}$$

and

$$\frac{1}{2\pi^{3/2}} \int_0^{\gamma} e^{r^2 t^2 - \frac{\mu^2}{4t^2}} \, \mathrm{d}t = \tag{5.30}$$

$$\frac{e^{-i\mu r}}{8\pi r} \left[-i + ie^{i2\mu r} \operatorname{erfc}\left(\frac{\mu}{2\gamma} + ir\gamma \right) + \operatorname{erfi}\left(r\gamma + i\frac{\mu}{2\gamma} \right) \right] \tag{5.31}$$

where $\operatorname{erf}(z)$ and $\operatorname{erfi}(z) = -i \operatorname{erf}(iz)$ are the error function and the imaginary error function (see e.g. [24]).

Now if we insert this into (5.27) we get

$$\frac{e^{-i\mu r}}{8\pi r} \Bigg\{ \left[1 - e^{i2\mu r} \left(1 + \operatorname{erf}\left(\frac{\mu}{2\gamma} + ir\gamma \right) \right) + i \operatorname{erfi}\left(r\gamma + i\frac{\mu}{2\gamma} \right) \right] - \tag{5.32}$$

$$i \left[-i + ie^{i2\mu r} \operatorname{erfc}\left(\frac{\mu}{2\gamma} + ir\gamma \right) + \operatorname{erfi}\left(r\gamma + i\frac{\mu}{2\gamma} \right) \right] \Bigg\} \tag{5.33}$$

If we do the cancellations this simplifies to

$$\frac{e^{-i\mu r}}{8\pi r} \left[-e^{i2\mu r} \left(1 + \operatorname{erf}\left(\frac{\mu}{2\gamma} + ir\gamma \right) + \operatorname{erfc}\left(\frac{\mu}{2\gamma} + ir\gamma \right) \right) \right] \tag{5.34}$$

We simplify this further by factoring out the exponential function inside the parenthesis and use $\operatorname{erf}(z) + \operatorname{erfc}(z) = \frac{2}{\sqrt{\pi}} \int_0^{\infty} e^{-\tau^2} \, \mathrm{d}\tau = 1$. We then end up

with

$$\frac{1}{4\pi}\frac{e^{-\mu r}}{r} \tag{5.35}$$

which is the analytic form of the free space Helmholtz kernel.

5.3 Numerical experiments

From Equation (5.27) we see that the entire real part of the integral is contained in the first term. Then from the second term we see that if we select γ sufficiently small compared to μ, this term can be neglected and the most significant contribution is contained within this integral. Thus we will approximate the Helmholtz by

$$H^{\mu}(r) \approx \frac{1}{2\pi^{3/2}} \int_0^{\infty} e^{-r^2(\gamma i - t)^2 + \frac{\mu^2}{4(\gamma i - t)^2}} \, \mathrm{d}t \tag{5.36}$$

Here we have some simple numerical experiments to illustrate how the kernel can be approximated accurately with an equispaced quadrature rule. The area we are trying to find accurate representations are set to $r \in [10^{-4}, \sqrt{3}]$. The choice of $\sqrt{3}$ is motivated by the fact that we require expansions to be valid within the three-dimensional interval $[0, 1]^3$, thus the longest possible distance between two points are $\sqrt{3}$. For the experiments here we select the step-size h in a similar manner as we did in chapter 4

$$h = \frac{1}{0.2 - 0.47 \log_{10}(\delta_0)} \tag{5.37}$$

only here the integrands can for some r and μ oscillate, introducing numerical difficulties. We circumvent this by selecting δ_0 less than the required error bound. This does increase the separation rank, but this is the price to pay for a separable representations of the Helmholtz kernel. Since γ only has to be chosen such that the last term in (5.27) is small enough, it can be selected to yield integrands that are relatively easy to integrate.

Since we need to evaluate the integrand over a finite area we look for mappings for t such that the integrand decays fast asymptotically. The most useful mapping we found was $t = \log\left(1 + e^{-\sinh(w)}\right) + \sinh(w)$. In Figures 5.1 - 5.2 we see examples of how the absolute relative error is bound in the area $r \in 10^{-4}, \sqrt{3}$. The error is easily controlled for small values of r. But we need a small step-size to keep the error bound for large values of r.

A case of interest is when μ gets small, which is displayed in Figure 5.3. As the real part of the integrand will get closer to the integrand of the Poisson kernel do we expect it to accurately be represented there, as can also be seen from the figure. However, if μ is small, the neglected term in (5.27) grow large, and we lose our accurate representation of the imaginary part. One fix to this is to reduce γ, but for this mapping the integrand gets too singular. A possible solution is to map the argument in (5.36) to $t = e^w$, this however yields a high separation rank, typically around $O(100)$. An alternative but maybe more viable approach would be to find a quadrature where the right hand side of the integral in (5.27) is accurately represented. Unfortunately we did not find any good candidates during the work of this thesis.

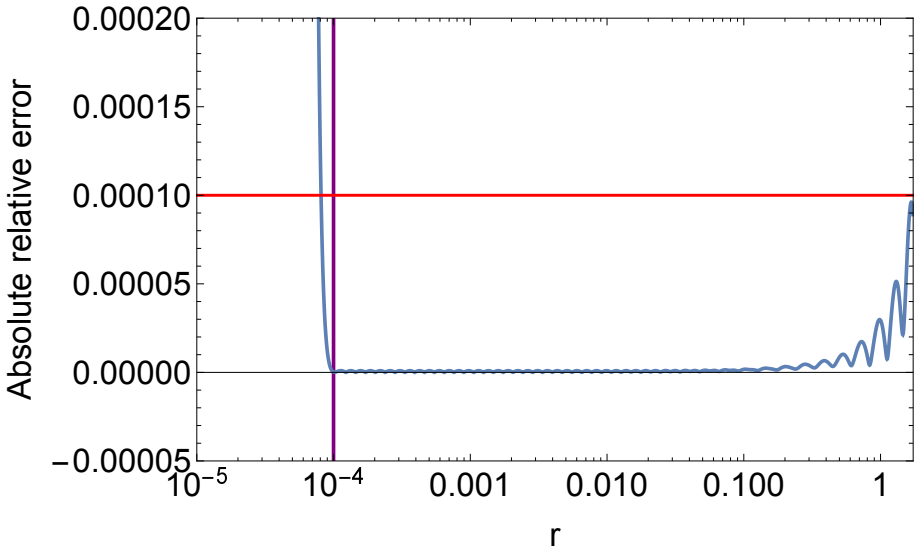

Figure 5.1: Plot of relative error $\left|H^{\mu}(r) - \tilde{H}^{\mu}(r)\right| / |H^{\mu}(r)|$ versus r. $r_{min} = 10^{-4}, r_{max} = \sqrt{3}$, $\mu = 4$, $\gamma = 0.7$, $\epsilon_s = 10^{-4}$ and $\delta_0 = 10^{-6}$. $w_0 = -4$, $w_M = 10.3$, $M = 45$. Error bound in red and minimum threshold r_{min} displayed in purple.

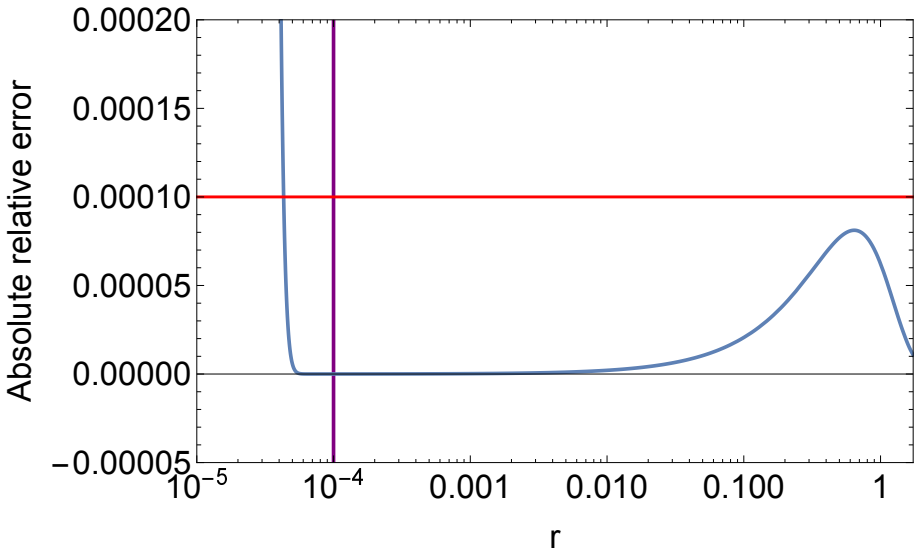

Figure 5.2: Plot of relative error $\left|H^{\mu}(r) - \tilde{H}^{\mu}(r)\right| / |H^{\mu}(r)|$ versus r. $r_{min} = 10^{-4}, r_{max} = \sqrt{3}$, $\mu = 10$, $\gamma = 1$, $\epsilon_s = 10^{-4}$ and $\delta_0 = 10^{-11}$. $w_0 = -4$, $w_M = 11.3$, $M = 84$. Error bound in red and minimum threshold r_{min} displayed in purple.

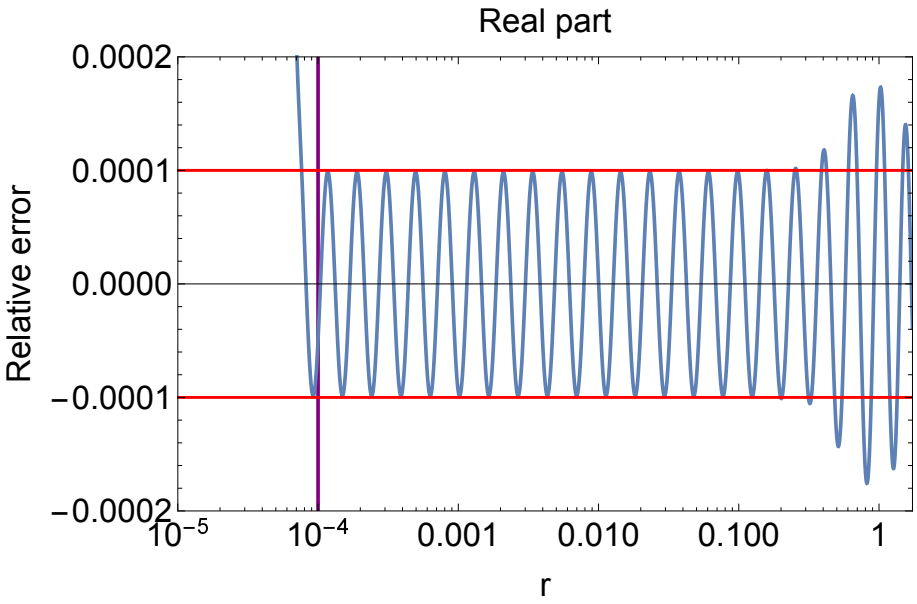

Figure 5.3: Plot of relative error $(Re[H^{\mu}(r)] - Re[\tilde{H}^{\mu}(r)])/Re[H^{\mu}(r)]$ versus r. $r_{min} = 10^{-4}, r_{max} = \sqrt{3}$, $\mu = 0.1$, $\gamma = 0.4$, $\epsilon_s = 10^{-4}$ and $\delta_0 = 10^{-4}$. $w_0 = -4$, $w_M = 10.3$, $M = 31$. Error bound in red and minimum threshold r_{min} displayed in purple.

6

Discussion

The purpose with this thesis was to investigate the possibility of reducing the separation rank for the separable representations of the Poisson and complex Helmholtz kernels, and look for a *feasible* separable representation of the (non-complex) Helmholtz kernel.

In both of these cases we succeeded, we found an easy method that proved successful in finding near optimal separation ranks for the Poisson and complex Helmholtz kernels.

In the second case we found a separable representation, that also, with some careful parameter choices and mappings can give us a separable representation of the Helmholtz kernel with a relatively small separation rank. However, for some cases the separation rank can be large (for instance for the imaginary part when μ is small). This means that for a large enough separation rank we risk the complexity of applying the separable version of the operator exceeds the complexity of directly applying it. But one must also remember that the storage requirement of separable integral kernels are *much* smaller than

kernels that has not been separated. Meaning operators that may not have been possible to efficiently store in a computer, can be stored efficiently, then by this reduce the computation time.

6.1 Future work

For the Poisson and complex Helmholtz kernels, there is not much to be done further, we are pretty much at an optimal configuration.

For the Helmholtz kernel, one can look for more optimal quadratures in the evaluation of the integrand as μ varies. Especially find an accurate method to evaluate the integral

$$\frac{1}{2\pi^{3/2}} \int_0^\gamma e^{r^2 t^2 - \frac{\mu^2}{4t^2}} \, \mathrm{d}t \tag{6.1}$$

accurately with a small separation rank, to achieve this the paper in reference [22] may prove helpful.

A

Bessel Functions

Bessel functions $y = y_\kappa(x)$ are solutions of the Bessel differential equation

$$\frac{\mathrm{d}^2 y}{\mathrm{d}x^2} + \frac{1}{x}\frac{\mathrm{d}y}{\mathrm{d}x} + \left(1 - \frac{\kappa^2}{x^2}\right) y = 0 \tag{A.1}$$

or equivalently

$$x^2 \frac{\mathrm{d}^2 y}{\mathrm{d}x^2} + x\frac{\mathrm{d}y}{\mathrm{d}x} + \left(x^2 - \kappa^2\right) y = 0 \tag{A.2}$$

where κ is a constant.

Special types of Bessel functions are what are called Bessel functions of the first kind $y = J_\kappa(x)$, Bessel functions of the second kind $y = Y_\kappa(x)$ (also called

Neumann functions and often written $y = N_\kappa(x)$), and Bessel functions of the third kind $y = H_\kappa^{(1)}(x) = J_\kappa(x) + iY_\kappa(x)$ and $y = H^{(2)_\kappa}(x) = J_\kappa(x) - iY_\kappa(x)$ (also called Hankel's functions). For more information see [25, 26]

A.1 Transformed Bessel differential equation

Following Bowman [27] we seek an equation satisfied by

$$y = x^\alpha y_\kappa(\beta x^\gamma) \tag{A.3}$$

where α, β and γ are constants. If we put

$$\eta = \frac{y}{x^\alpha} \qquad\qquad \xi = \beta x^\gamma \tag{A.4}$$

then (A.3) gives $\eta = J_\kappa(\xi)$, hence

$$\xi^2 \frac{\mathrm{d}^2\eta}{\mathrm{d}\xi^2} + \xi \frac{\mathrm{d}\eta}{\mathrm{d}\xi} + (\xi^2 - \kappa^2)\eta = 0 \tag{A.5}$$

and since

$$\xi \frac{\mathrm{d}}{\mathrm{d}\xi}\left(\xi \frac{\mathrm{d}\eta}{\mathrm{d}\xi}\right) = \xi^2 \frac{\mathrm{d}^2\eta}{\mathrm{d}\xi^2} + \xi \frac{\mathrm{d}\eta}{\mathrm{d}\xi} \tag{A.6}$$

then (A.5) can be written

$$\xi \frac{\mathrm{d}}{\mathrm{d}\xi}\left(\xi \frac{\mathrm{d}\eta}{\mathrm{d}\xi}\right) + (\xi^2 - \kappa^2)\eta = 0 \tag{A.7}$$

by the chain rule

$$\frac{\mathrm{d}\eta}{\mathrm{d}\xi} = \frac{\mathrm{d}\eta}{\mathrm{d}x}\frac{\mathrm{d}x}{\mathrm{d}\xi} \tag{A.8}$$

where

$$\frac{\mathrm{d}x}{\mathrm{d}\xi} = \frac{1}{\gamma\beta}\left(\frac{\xi}{\beta}\right)^{\frac{1}{\gamma}-1} = \frac{x}{\xi} \tag{A.9}$$

therefore

$$\xi\frac{\mathrm{d}\eta}{\mathrm{d}\xi} = \frac{x}{\gamma}\frac{\mathrm{d}\eta}{\mathrm{d}\xi} \tag{A.10}$$

then

$$\xi\frac{\mathrm{d}}{\mathrm{d}\xi}\left(\xi\frac{\mathrm{d}\eta}{\mathrm{d}\xi}\right) = \frac{x}{\gamma^2}\frac{\mathrm{d}}{\mathrm{d}x}\left(x\frac{\mathrm{d}\eta}{\mathrm{d}\xi}\right) \tag{A.11}$$

follows immediately. Next using the product rule we find

$$x\frac{\mathrm{d}\eta}{\mathrm{d}x} = x\frac{\mathrm{d}}{\mathrm{d}x}yx^{-\alpha} = \frac{1}{x^{\alpha-1}}\frac{\mathrm{d}y}{\mathrm{d}x} - \frac{\alpha}{x^{\alpha}} \tag{A.12}$$

again using the product rule we find

$$x\frac{\mathrm{d}}{\mathrm{d}x}\left(x\frac{\mathrm{d}\eta}{\mathrm{d}x}\right) = \frac{1}{x^{\alpha-2}}\frac{\mathrm{d}^2y}{\mathrm{d}x^2} - \frac{2\alpha-1}{x^{\alpha-1}}\frac{\mathrm{d}y}{\mathrm{d}x} + \frac{\alpha^2}{x^{\alpha}} \tag{A.13}$$

hence the equation satisfied by y is

$$\frac{1}{\gamma^2}\left(\frac{1}{x^{\alpha-2}}\frac{\mathrm{d}^2y}{\mathrm{d}x^2}-\frac{2\alpha-1}{x^{\alpha-1}}\frac{\mathrm{d}y}{\mathrm{d}x}+\frac{\alpha^2}{x^\alpha}y\right)+\left(\frac{\beta^2x^{2\gamma}-\kappa^2}{x^\alpha}\right)y=0 \tag{A.14}$$

or

$$\frac{\mathrm{d}^2y}{\mathrm{d}x^2}-\frac{2\alpha-1}{x}\frac{\mathrm{d}y}{\mathrm{d}x}+\left(\beta^2\gamma^2x^{2\gamma-2}+\frac{\alpha^2-\kappa^2\gamma^2}{x^2}\right)y=0 \tag{A.15}$$

with corresponding general solutions

$$y=x^\alpha\left[AJ_\kappa(\beta x^\gamma)+BY_\kappa(\beta x^\gamma)\right] \tag{A.16}$$

$$\tag{A.17}$$

A case of particular interest to us is when $\alpha=-\frac{1}{2}$, $\kappa=\frac{1}{2}$, $\gamma=1$ and $\beta=\pm\mu$ where μ is a positive real constant, then (A.15) reveal itself as

$$\frac{\mathrm{d}^2y}{\mathrm{d}x^2}+\frac{2}{x}\frac{\mathrm{d}y}{\mathrm{d}x}+\mu^2y=0 \tag{A.18}$$

the corresponding general solution (A.16) then takes the form

$$y=x^{-\frac{1}{2}}\left[AJ_{\frac{1}{2}}(\pm\mu x)+BY_{\frac{1}{2}}(\pm\mu x)\right] \tag{A.19}$$

using [23] we find

$$J_{\frac{1}{2}}(\pm\mu)=\sqrt{\frac{2}{\mu\pi}}\frac{\sin(\mu x)}{x^{\frac{1}{2}}} \tag{A.20}$$

and

$$Y_{\frac{1}{2}}(\pm\mu) = \sqrt{\frac{2}{\mu\pi}}\frac{\cos(\mu x)}{x^{\frac{1}{2}}} \tag{A.21}$$

with this we select $A' = iA\sqrt{\frac{2}{\mu\pi}} = B\sqrt{\frac{2}{\mu\pi}}$, and with Euler's identity [28] a solution to (A.18) is

$$y^{\pm}(x) = A'\frac{e^{\pm i\mu x}}{x} \tag{A.22}$$

A equally relevant case for us is when $\alpha = -\frac{1}{2}$, $\kappa = \frac{1}{2}$, $\gamma = 1$ and $\beta = \pm i\mu$ where μ is a positive real constant and i is the imaginary unit. Now (A.15) transforms into

$$\frac{\mathrm{d}^2y}{\mathrm{d}x^2} + \frac{2}{x}\frac{\mathrm{d}y}{\mathrm{d}x} - \mu^2 y = 0 \tag{A.23}$$

with corresponding solutions

$$y = x^{-\frac{1}{2}}\left[AJ_{\frac{1}{2}}(\pm i\mu x) + BY_{\frac{1}{2}}(\pm i\mu x)\right] \tag{A.24}$$

using [23] and selecting A in a similar way as we did in the previous case we find

$$J_{\frac{1}{2}}(\pm\mu) = A\frac{\sinh(\pm\mu x)}{x^{\frac{1}{2}}} \tag{A.25}$$

and

$$Y_{\frac{1}{2}}(\pm\mu) = A\frac{\cosh(\pm\mu x)}{x^{\frac{1}{2}}} \tag{A.26}$$

This combined with the identity $\cosh(x) + \sinh(x) = \frac{e^x+e^{-x}}{2} + \frac{e^x-e^{-x}}{2} = e^x$ equation (A.24) takes the form

$$y^{\pm}(x) = A\frac{e^{\pm\mu x}}{x} \tag{A.27}$$

B

Rotational invariance of the homogenous Laplace, complex Helmholtz and Helmholtz equations

The content here is from [29], and expanded to be valied for the complex Helmholtz and Helmholtz equation.

An equation is rotationally invariant if the equation does not change under rotations around some point. Here we show how Rotational invariance of $\mathcal{L}u = 0$, that is, if A is an orthogonal $n \times n$ where the matrix elements are denoted a_{ij}.

We define

$$v(x) = u(Ax) \tag{B.1}$$

$$D_i v(x) = \sum_{k=1}^{n} D_k u(Ax) a_{ki} \tag{B.2}$$

$$D_i j v(x) = \sum_{l=1}^{n} \sum_{k=1}^{n} D_{kl} u(Ax) a_{ki} a_{lj} \tag{B.3}$$

Since A is orthogonal, then $AA^T = I$ where I is the $n \times n$ identity matrix, and T denotes the transpose. Thus for all $k, l = 1, ..., n$

$$(\nabla^2 + c)v(x) = \sum_{i=1}^{n} \sum_{l=1}^{n} \sum_{k=1}^{n} D_{kl} u(Ax) a_{ki} a_{lj} + cu(Ax) \tag{B.4}$$

$$= \sum_{l=1}^{n} \sum_{k=1}^{n} D_{kl} u(Ax) \left(\sum_{i=1}^{n} a_{ki} a_{li} \right) cu(Ax) \tag{B.5}$$

$$= \sum_{l=1}^{n} \sum_{k=1}^{n} D_{kl} u(Ax) \left(\sum_{i=1}^{n} \delta_{kl} \right) cu(Ax) \tag{B.6}$$

$$= (\nabla^2 + c)u(Ax) = 0 \tag{B.7}$$

That is

$$(\nabla^2 + c)v(x) = (\nabla^2 + c)u(Ax) = 0 \tag{B.8}$$

thus The homogenous Laplace, complex Helmholtz and Helmholtz equation are rotationally invariant.

Bibliography

[1] Multiresolution chemistry (mrchem) program package. See http://mrchemdoc.readthedocs.org/en/latest/, 2016.

[2] Walter Kohn and Lu Jeu Sham. Self-consistent equations including exchange and correlation effects. *Physical review*, 140(4A):A1133, 1965.

[3] Pierre Hohenberg and Walter Kohn. Inhomogeneous electron gas. *Physical review*, 136(3B):B864, 1964.

[4] John P Perdew, Karla Schmidt, V Van Doren, C Van Alsenoy, and P Geerlings. Jacob's ladder of density functional approximations for the exchange-correlation energy. In *AIP Conference Proceedings*, volume 577, pages 1–20. AIP, 2001.

[5] Bradley K Alpert. A class of bases in l^2 for the sparse representation of integral operators. *SIAM journal on Mathematical Analysis*, 24(1):246–262, 1993.

[6] Gregory Beylkin, Vani Cheruvu, and Fernando Pérez. Fast adaptive algorithms in the non-standard form for multidimensional problems. *Applied and Computational Harmonic Analysis*, 24(3):354–377, 2008.

[7] Fritz John. *Partial differential equations, volume 1 of Applied Mathematical Sciences*. Springer-Verlag, New York,, 1982.

[8] Arnold Sommerfeld. *Partial differential equations in physics*, volume 1.

Academic press, 1949.

[9] Luca Frediani, Eirik Fossgaard, Tor Fla, and Kenneth Ruud. Fully adaptive algorithms for multivariate integral equations using the non-standard form and multiwavelets with applications to the poisson and bound-state helmholtz kernels in three dimensions. *Molecular Physics*, 111(9-11):1143–1160, 2013.

[10] Robert J Harrison, George I Fann, Takeshi Yanai, and Gregory Beylkin. Multiresolution quantum chemistry in multiwavelet bases. In *International Conference on Computational Science*, pages 103–110. Springer.

[11] Wolfgang Hackbusch and Boris N Khoromskij. Low-rank kronecker-product approximation to multi-dimensional nonlocal operators. part i. separable approximation of multi-variate functions. *Computing*, 76(3-4):177–202, 2006.

[12] Gregory Beylkin, Christopher Kurcz, and Lucas Monzón. Fast convolution with the free space helmholtz green's function. *Journal of Computational Physics*, 228(8):2770–2791, 2009.

[13] Paul P Ewald. Die berechnung optischer und elektrostatischer gitterpotentiale. *Annalen der Physik*, 369(3):253–287, 1921.

[14] Gregory Beylkin, Christopher Kurcz, and Lucas Monzón. Grids and transforms for band-limited functions in a disk. *Inverse Problems*, 23(5):2059, 2007.

[15] Gregory Beylkin and Lucas Monzón. Approximation by exponential sums revisited. *Applied and Computational Harmonic Analysis*, 28(2):131–149, 2010.

[16] Gregory Beylkin. On the fast fourier transform of functions with singularities. *Applied and Computational Harmonic Analysis*, 2(4):363–381,

1995.

[17] Alok Dutt and Vladimir Rokhlin. Fast fourier transforms for nonequispaced data. *SIAM Journal on Scientific computing*, 14(6):1368–1393, 1993.

[18] Leslie Greengard and June-Yub Lee. Accelerating the nonuniform fast fourier transform. *SIAM review*, 46(3):443–454, 2004.

[19] June-Yub Lee and Leslie Greengard. The type 3 nonuniform fft and its applications. *Journal of Computational Physics*, 206(1):1–5, 2005.

[20] Paul Peter Ewald. *Dispersion und Doppelbrechung von Elektronengittern (Kristallen)*. Dieterichschen Universitats-Buchdruckerei, 1912.

[21] Erich Zauderer. *Partial differential equations of applied mathematics*, volume 71. John Wiley & Sons, 2011.

[22] Gregory Beylkin and Lucas Monzon. On generalized gaussian quadratures for exponentials and their applications. *Applied and Computational Harmonic Analysis*, 12(3):332–373, 2002.

[23] Wolfram Research, Inc. *Mathematica Version 11.0*, 2016.

[24] Milton Abramowitz and Irene A Stegun. *Handbook of mathematical functions: with formulas, graphs, and mathematical tables*, volume 55. Courier Corporation, 1964.

[25] Izrail Solomonovich Gradshteyn and Iosif Moiseevich Ryzhik. *Table of integrals, series, and products*. Academic press, 2014.

[26] Milton Abramowitz and Irene A Stegun. *Handbook of mathematical functions: with formulas, graphs, and mathematical tables*, volume 55. Courier Corporation, 1964.

[27] Frank Bowman. *Introduction to Bessel functions*. Courier Corporation, 2012.

[28] Leonhard Euler. Leonhardi euleri opera omnia. 1, opera mathematica. volumen viii, leonhardi euleri introductio in analysin infinitorum. tomus primus/ediderunt adolf krazer et ferdinand rudio. 1922.

[29] Rotational invariance laplace equation. http://www.math.wisc.edu/ feldman/819/sol1.pdf. Accessed: 2017-02-02.